The role of inhibitory neurons in novelty sound detection in regular and random statistical contexts.

Xiaomao Ding[1,2], Nathan W. Vogler[1], Melanie Tobin[1], Linda Garami[1], Katherine C. Wood[1,3], Maria N. Geffen[1,2]

1. Department of Otorhinolaryngology, University of Pennsylvania, Philadelphia, PA, USA

2. Neuroscience Graduate Group, University of Pennsylvania, Philadelphia, PA, USA

3. University of Sheffield, Sheffield UK

*Corresponding author:

Maria Neimark Geffen, Ph.D. (she/her)

Department of Otorhinolaryngology

Perelman School of Medicine

University of Pennsylvania

5 Ravdin

3400 Spruce St.

Philadelphia PA 19104

Tel.: 215.898.0782

ABSTRACT

Detecting statistical regularities in sound and responding to violations of these patterns, termed novelty detection, is a core function of the auditory system. Human studies have shown that novelty responses are enhanced in regular compared to random auditory contexts, but the underlying circuit mechanisms remain unclear. Here, we examined how inhibitory neurons contribute to context-dependent novelty responses in mouse auditory cortex. Using two-photon calcium imaging in the auditory cortex of awake head-fixed male and female mice, we recorded neuronal activity during presentation of spectro-temporally rich ripple sounds, with novel ripples embedded in either regular or random ripple sequences. AC neurons exhibited enhanced responses to novel sounds in regular contexts compared to random ones. To identify circuit mechanisms, we selectively inactivated parvalbumin (PV), somatostatin (SST), or vasoactive intestinal polypeptide (VIP) inhibitory neurons using optogenetics during imaging. Inactivation of PV and SST neurons broadly increased novelty responses in both contexts. In contrast, VIP inactivation selectively reduced responses to novel stimuli in the regular context, abolishing the context-dependent enhancement. At the population level, inactivating all three neuronal subtypes increased detectability of the novel stimulus, but with VIP inactivation, the shift was stronger for regular than random context. These findings reveal a distinct role for VIP neurons in modulating prediction error signals based on temporal structure, suggesting that VIP circuits are critical for context-sensitive auditory processing.

INTRODUCTION

Successfully navigating everyday sound environments requires the auditory system to detect and interpret predictable and unexpected patterns (Barascud et al., 2016; Sohoglu and Chait, 2016; Parras et al., 2017; Southwell and Chait, 2018). Natural sounds are characterized not only by their spectral content but also by higher-order spectro-temporal regularities: statistical structures that allow listeners to form predictions about upcoming auditory events. Detecting violations of these predictions—referred to as *novelty detection*—is a core auditory computation. These computations support a wide range of behaviors, from identifying a familiar voice in a noisy crowd to detecting an approaching vehicle amid ambient noise (Arnal and Giraud, 2012). Extensive research in humans and non-human animals has demonstrated that the brain encodes both predictions and prediction errors, with signals such as the mismatch negativity (MMN) reflecting changes in neural activity in response to unexpected sounds (Naatanen et al., 1978, 2004, 2007). Novelty signals have been observed across multiple stages of the auditory pathway, including the inferior colliculus (IC) (Lesicko et al., 2022), medial geniculate body (MGB) (Antunes et al., 2010; Malmierca et al., 2015), and auditory cortex (AC) (Nelken, 2004, 2014; Hershenhoren et al., 2014; Natan et al., 2015, 2017; Rubin et al., 2016; Parras et al., 2017). However, the transformations of prediction and deviance signals along this pathway, and the neural mechanisms that shape their context sensitivity, remain incompletely understood.

Recent studies in humans have shown that novelty responses are enhanced when novel sounds are embedded within regular, predictable contexts as compared to random ones (Sohoglu and Chait, 2016; Southwell and Chait, 2018). For example, a regular context may consist of a repeating sound sequence (e.g., ABCD, ABCD…), whereas a random context involves the same elements shuffled in order (e.g., BADC, ADCB…). Stronger responses to a novel sound X

following a regular pattern suggest that the brain not only detects violations in the global structure of sound, but also modulates prediction strength based on contextual, local structure. Whereas EEG studies point to AC as the center for the context-dependent novelty responses, how these responses are created at individual neuronal and circuit level remains unknown. Nearly all neurons in AC show adaptation to frequently presented sounds and an enhanced response to rare, deviant stimuli (Harms et al., 2014; Parras et al., 2017) — a phenomenon known as stimulus-specific adaptation (SSA) (Ulanovsky et al., 2003; Szymanski et al., 2009; Farley et al., 2010; Natan et al., 2015). Furthermore, studies have shown that AC neurons are also sensitive to patterns with structure across multiple time scales (Ulanovsky et al., 2004; Yaron et al., 2012; Mehra et al., 2022). Here, we asked whether individual AC neurons exhibit enhanced novelty responses in regular as compared to random context, and whether intra-cortical inhibitory-excitatory circuits support this transformation.

Inhibitory neurons in AC play distinct roles in shaping auditory cortical responses to sound patterns. The two most common subtypes, parvalbumin (PV)- and somatostatin (SST)-neurons (Lee et al., 2010; Tremblay et al., 2016; Wood et al., 2017), differentially contribute to SSA and other forms of auditory adaptation (Levy and Reyes, 2012; Chen et al., 2015; Natan et al., 2015, 2017; Phillips et al., 2017), while another prominent subtype, vasoactive intestinal polypeptide (VIP)-expressing neurons, contribute to context- and state-dependent modulation in multiple cortical areas (Lee et al., 2010; Tremblay et al., 2016; Wood et al., 2017). VIP neurons, in particular, have been proposed to gate top-down influences and modulate predictive coding processes through a disinhibitory circuit. We hypothesized that these distinct inhibitory neuron classes differentially contribute to novelty detection depending on regular or random context.

Using two-photon calcium imaging in awake mice, we recorded neuronal activity of large populations of neurons in auditory cortex during presentation of novel spectro-temporally complex ripple stimuli embedded in either regular or random sound contexts. We combined imaging with optogenetic inactivation of PV, SST, or VIP neurons to determine their respective roles in modulating novelty responses.

We found that regular context enhanced novelty responses compared to random context, and that this enhancement was differentially shaped by inhibitory neuron class. PV and SST inactivation increased responses to novel sounds, but the role of context was non-specific, whereas VIP inactivation selectively reduced novelty responses in the regular, but not random context. At the population level, VIP inactivation eliminated the contextual enhancement of novelty detection, implicating VIP neurons as a key component of the circuit that integrates statistical structure to shape novelty responses.

METHODS

Animals

A total of 14 mice (male/female) were used in this study. The strains used were: Cdh23 x PV-Cre (B6.CAST-Cdh23Ahl+/Kjn, JAX: 002756 x Pvalbtm1(cre)Arbr/J, JAX: 017320; n = 4), Cdh23xSST-Cre (B6.CAST-Cdh23Ahl+/Kjn x Ssttm2.1(cre)Zjh/J, 113 JAX: 013044; n = 4), VIP-IRES-Cre (B6.CAST-Cdh23Ahl+/Kjn x Viptm1(cre)Zjh/J, JAX: 010908; n = 3), VGAT-Cre crossed with transgenic GCaMP8m (Slc32a1tm2(cre)Lowl/J, JAX: 016962 x Igs7tm1(tetO-GCaMP8m,CAG-tTA2)Genie/J, JAX:037718, n = 3), Cdh23 (B6N(Cg)-Cdh23tm2.1Kjn/Kjn, n = 5), aged 12-26 weeks. Cdh23 mice were used because they do not exhibit age-related hearing loss which is common in C57BL/6J mice (Johnson et al., 2017). Mice were housed individually after

cranial window implant and were housed on a reversed light-dark cycle. Experimental procedures were performed in accordance with NIH guidelines and approved by the IACUC at the University of Pennsylvania.

Surgery Procedures

Cranial window implants were implanted following a procedure described previously (Wood et al., 2022; Tobin et al., 2024). Mice were anesthetized with 3% isoflurane which was steadily reduced to 1.5% through the surgery. A 3 mm craniotomy was performed over the left auditory cortex with a 3 mm biopsy punch. A viral 750 nL cocktail (4:1 ratio) of GCAMP (7f: AAV1-Syn-jGCaMP7f-WPRE, Addgene 104488 or 8m: pGP-AAV-syn-jGCaMP8m-WPRE, Addgene 162375) and JAWS (AAV8-CAG-FLEX-JAWS-kgc-tdTomato, UNC Vector Core or AAV8-CAG-FLEX-JAWS-kgc-tdTomato, Penn Vector Core, Addgene 84446) was injected at 3 locations in the craniotomy, separated 0.3-0.5 mm apart in the anterior-posterior direction. The craniotomy was then sealed with a custom round glass window consisting of a 3 mm window glued to a 4 mm window with Norland Optical Adhesive 68. A custom-made metal headplate was attached to the skull with C&B Metabond dental cement. For transgenic GCaMP8m mice, no virus was injected and only the window implant was performed. Mice were allowed to recover for 3 weeks before imaging started.

Two-photon imaging

All imaging sessions were performed in a custom-built acoustic isolation booth using previously published methods (Betzel et al., 2019; Wood et al., 2022; Tobin et al., 2024). Mice were habituated to being head fixed for 3 days prior to imaging. Wide-field imaging was performed on each mouse

to identify sound-responsive areas of the window before two-photon imaging. We imaged in layer 2/3 of auditory cortex of awake head-fixed mice using a two-photon microscope (Ultima 2Pplus *in vivo* multiphoton microscope, Bruker) with a 940 nm laser (Chameleon Ti-Sapphire) with a 16X Nikon objective with a 0.8 numerical aperture (Thorlabs, N16XLWD-PF) (Figure 1 A, B, D). Recordings were made at 512 x 512 pixels and at 30 frames per second.

Optogenetic Manipulation

Optogenetic stimulation was performed using a LED (Thorlabs M625L4) delivering 625 nm light through the objective lens (Tobin et al., 2024). Before each stimulus session, the LED light power was calibrated to ~2.8 mW/mm^2 for mice injected with the JAWS from the Penn Vector Core and ~7 mW/mm^2 for mice injected with Jaws from the UNC Vector Core based on reported inhibition performance of JAWS (Chuong et al., 2014). Optogenetic manipulation occurred randomly in 50% of presentations of the novel ripple. The LED was turned on continuously for 300 ms, synced with stimulus onset, during the novel ripple presentation.

Acoustic stimuli

Auditory moving ripples were generated at a sampling rate of 400 kHz in MATLAB according to the following formula:$S(t,x) = L[1 + \Delta A sin(2\pi wt + 2\pi\Omega x + \Phi)]$

where w is the temporal modulation parameter and Ω is the spectral modulation parameter. Individual ripples spanned a frequency range of 5-50 kHz, lasted 300 ms, were presented at 70 dB SPL with a 15 dB modulation depth, and had a 5 ms cosine ramp applied at the beginning and end. Background sequences were generated by concatenating ripples A, B, C, and D in either a fixed sequence (REG) or a random sequence (RND) resulting in a 1.2 s stimulus (Figure 1C). The novel

sequence was generated by concatenating ripples X, Y, Z, and W in that order for all stimulus conditions. Sequences were presented with a 1 s inter-stimulus interval. Background sequences were repeated 3-6 times pseudo-randomly before a novel sequence was presented. A control sequence of each ripple presented in isolation with a 1 s ISI was also presented to determine the base sound response of neurons.

Electrophysiology

Mice were prepared for *in vivo* electrophysiological recordings as described previously (Vogler et al., 2024). At least two weeks prior to recordings, a ground pin was inserted via small craniotomy over the left frontal cortex, and a custom-made stainless steel headplate (eMachine Shop) was secured to the skull using dental cement (C&B Metabond) and acrylic (Lang Dental) (Vogler et al., 2024). Recordings were performed in a custom-built acoustic isolation booth. At least one week following headplate surgery, mice were habituated to the recording setup for increasing durations (5-60 min) over the course of 3 days. On the day of recording, mice were anesthetized with 1.5-2.5% isoflurane, and a small craniotomy was made over the left auditory cortex using a dental drill, centered ~1.5mm anterior to the lambdoid suture along the caudal end of the squamosal suture. Following the craniotomy, mice were allowed to recover from anesthesia for at least 30 min. Acute extracellular recordings in the auditory cortex were performed using a 32-channel silicon probe (A1x32-Poly2-5mm-50s-177, NeuroNexus). The probe was positioned perpendicularly to the brain surface and lowered at 1-2 um/s to a final depth of 900-1200 um or until all channels were within the brain. During lowering of the probe, we monitored responses to brief broadband noise clicks to confirm localization within auditory cortex. Neuronal signals were amplified and digitized with an Intan headstage (RHD 32ch) and recorded by an OpenEphys

acquisition board (Siegle et al., 2017) at a rate of 30 kHz. Signals were filtered between 500 and 6000 Hz, offset corrected, and re-referenced to the median across all channels. Spiking data were sorted using Kilosort2 (Pachitariu et al., 2016) and manually curated in phy2 to identify putative single- and multi-units.

Data analysis and statistics

Suite2P (Pachitariu et al., 2017) was used to register raw two-photon images, select regions of interest (ROI), and perform neuropil correction (Betzel et al., 2019; Wood et al., 2022; Tobin et al., 2024). A 0.3 Hz highpass filter was used to correct for slow fluctuations in the calcium signal. The calcium signal from each ripple sequence was converted to a z-scored $\Delta F/F_{std}=(F-mean(F_{baseline}))/std(F_{baseline})$ where $F_{baseline}$ is the calcium signal from the 300 ms preceding stimulus onset. An additional motion correction step was performed using PatchWarp (Hattori and Komiyama, 2022). We found that small motion artifacts during imaging induced negative transients in the calcium trace. These artifacts were identified by setting a threshold for the X and Y values from the summary stat output and any trials within 3 frames of an artifact were removed from further analysis. This removed approximately 10% of all trials recorded.

For statistical comparison of responses, we computed the mean response strength during the 300 ms following the onset of a ripple on each trial. To identify neurons exhibiting significant novelty responses, we compared the responses over trials during the same ripple presented as novel and tuning stimulus using an unpaired t-test in either random or regular context. To compare novelty response strength across neurons in different conditions, we computed mean response to the first ripple X in the novel stimulus sequence and implemented repeated measures ANOVA with context (regular or random) and light (on or off) as two factors. We used Tukey-Kramer for post-hoc

comparisons. If the output of the statistical test in MATLAB resulted in "p = 0", this was most likely due to a rounding error and we reported it as $p < 1e\text{-}10$.

Exponential Fits

Mean responses y from 0-300 ms after stimulus onset for individual trials were fit to the exponential function below:

$$y = a * e^{bx} + c$$

The variables a, b, and c were free parameters, and the variable x represented the trial presentation number. A neuron was considered to have a significant adaptation effect ($a > 0$) or facilitation effect ($a < 0$) if the RMSE from the exponential fit was less than the RMSE to the mean response. Fits were performed using MATLAB's curve fitting toolbox.

SVM

Sample populations of neurons were selected by bootstrapping either 1, 12, 25, 50, 100, or 200 neurons from within a single recording session. For each sample, the population response was represented as a vector with each entry being the mean response of a neuron from 0-300 ms from stimulus onset for an individual trial. Then, a support vector machine (SVM) was trained to predict either ripple identity from the tuning stimulus or background context (REG/RND) from the novelty stimulus (Vapnik, 2013; Wood et al., 2022; Tobin et al., 2024). 20% of the trials were held out as a test set while the SVM was trained on the remaining 80%. For each population size, sample neuronal responses were bootstrapped 1000 times. Results presented represent the mean prediction performance across 1000 models for the specified population size.

RESULTS

Characterizing the sound response to individual moving ripples

We imaged calcium activity in populations of neurons in layer 2/3 of auditory cortex (AC) in awake, head-fixed mice presented with a series of sequences of spectrotemporally complex sounds (termed “ripples”) (Figure 1 A-D). Each ripple was comprised of a broadband sound with the envelope and frequency modulation varying in time. For the regular (REG) and random (RND) background ripples, we used the same 4 ripples (300 ms long, 5-50 kHz, 70 dB SPL mean intensity), which were repeated in the same sequence (REG; ABCD, ABCD, ABCD, …), or in varying order (RND; BADC, BDAC, CBDA, …). Each background sequence consisted of 3-6 repeats of the 4 ripples with 1 s inter-repeat interval followed by the novel ripple sequence. Because the background sequence is comprised of the same ripples in both REG and RND, the only difference between the two contexts is the temporal order. The novel sequence of ripples included 4 different ripples from those used in the background. These ripples were in the same frequency range but had different modulation frequencies. Additionally, the ripples were also presented individually with a 1 sec interstimulus interval to construct baseline tuning responses.

This stimulus allowed us to test multiple aspects of the neuronal responses to sounds in varying statistical regimes. First, we tested whether a given ripple evoked a greater or smaller neuronal response when it was unexpected. Second, we tested whether a novel ripple elicited a greater or smaller response in the regular or random context. Third, we tested whether the responses to the context ripples differed when they were presented in regular or random context, and whether adaptation to their presentation over subsequent repeats differed based on whether their order was regular or random. We expected the responses to novel ripples to be greater than the respective baseline sound response. We also expected novelty responses to be greater in the

regular than random context. Finally, we expected adaptation to repeated ripple sequences to be stronger for regular than random contexts.

We recorded activity from 9,126 neurons in the AC, with 77.3% (n = 7,054) showing a significant sound response to at least one ripple (z-scored averaged fluorescent response 0-300 ms post stimulus-onset versus the average fluorescence 0-300 ms before stimulus on each trial, t-test with a Bonferroni correction for the number of ripples). The fluorescence of neurons typically increased over the first 200 ms after sound presentation followed by a gradual decrease in fluorescence (representative neurons, Figure 1E). Across all imaged neurons, 21.9% (n = 2,000/9,126) responded to only one ripple while 6.1% (n = 557/9,126) had significant responses to all eight ripples. Additionally, the distribution of responsive neurons by ripple was relatively even across all eight ripples, with a maximum difference in response rate of 10.2% (Figure 1 F, G). Whereas many neurons exhibited an enhancement in fluorescence in response to the ripples (n = 2,127/7,054), the majority of imaged neurons exhibited a suppression in fluorescence to individual ripples (n = 4,927/7,054, Figure 1H). The suppression in fluorescence corresponds to a decrease in calcium concentration, which most likely is due to reduced spiking activity in response to the moving ripples (Attinger et al., 2017; Solyga and Keller, 2025). When appropriate, we analyzed the enhanced responses as a separate group from suppressed responses. Combined, responses to individual ripples demonstrate that these stimuli efficiently drive neuronal calcium responses in AC.

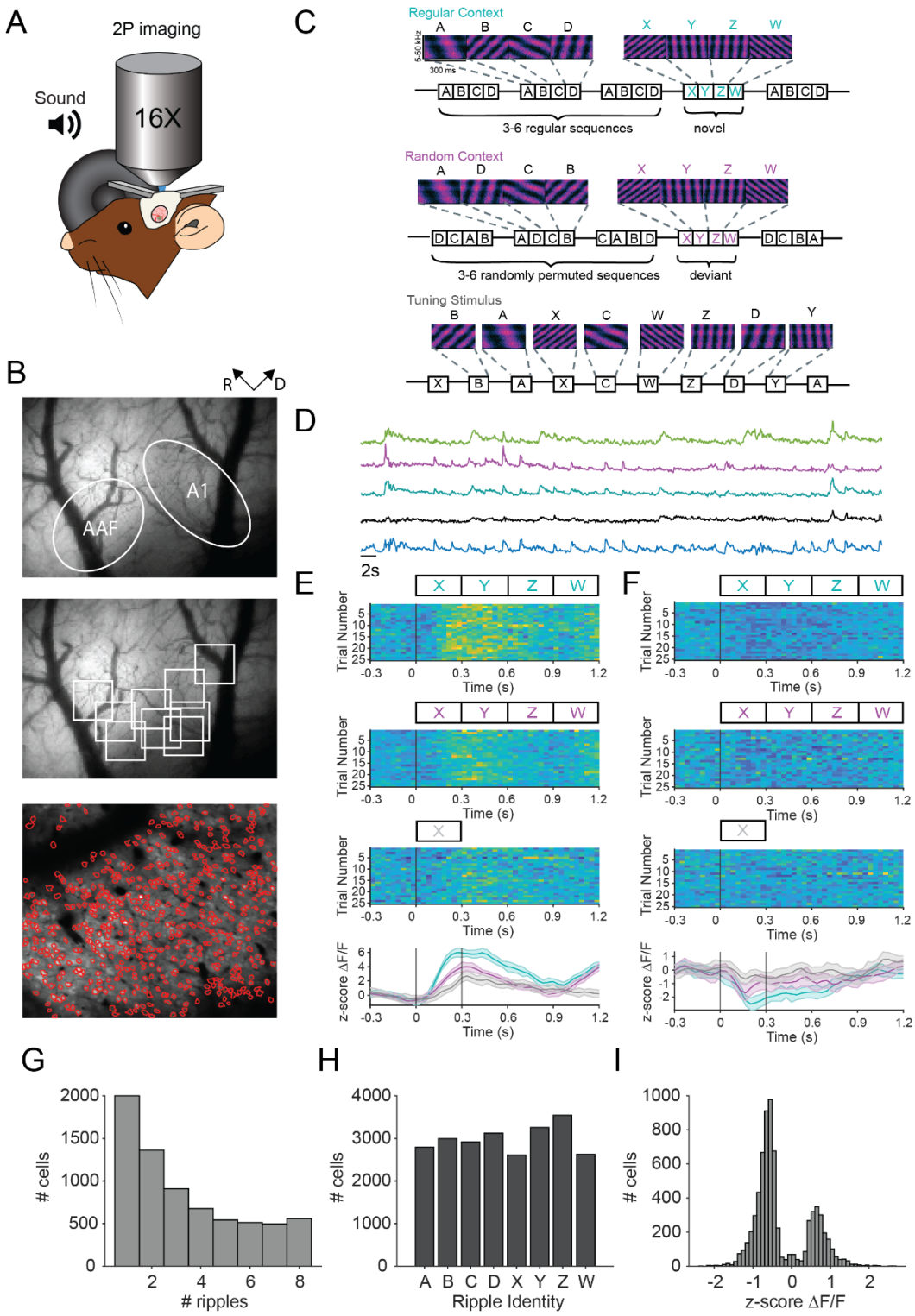
A
2P imaging
Sound
16X
B
R
D
AAF
A1
C
Regular Context
A B C D
X Y Z W
5-50 kHz
300 ms
A B C D A B C D A B C D X Y Z W A B C D
3-6 regular sequences
novel
Random Context
A D C B
X Y Z W
D C A B A D C B C A B D X Y Z W D C B A
3-6 randomly permuted sequences
deviant
Tuning Stimulus
B A X C W Z D Y
X B A X C W Z D Y A
D
2s
E
F
X Y Z W
Trial Number
Time (s)
z-score ΔF/F
G
cells
ripples
H
Ripple Identity
A B C D X Y Z W
I
z-score ΔF/F

FIGURE 1

a Schematic of two-photon calcium imaging setup. **b** Widefield image from an example mouse with identified areas for A1 and anterior auditory field (AAF) regions (top). Recording sites across different mice mapped onto the example widefield image (middle). Example 2P imaging site with ROIs circled in red (bottom). **c** Moving ripples used in the experiment and stimulus schematic. Ripples spanned from 5-50 kHz and were 300 ms long in duration. Regular sequences had a fixed temporal pattern while random sequences shuffled the background ripple order. The novel stimulus (novel) sequence was the same for both conditions. **d** Example 2P calcium traces from 5 neurons from the same recording session. **e,f** Responses over the successive trials and mean response trace to the novel ripple in regular (top/purple) and random (middle/ctab) contexts as well as the same ripple in the tuning sequence (bottom/gray) from example cells with a positive response (e) and a negative response (f). Shaded error bars represent SEM. **g** Distribution of neurons responsive to only 1 ripple up to all 8 ripples. A significant response was determined with a t-test of the mean response from 0-300 ms post-stimulus a $p < 0.05$ with a Bonferroni correction. **h** Distribution of neurons responsive to specific ripples. **i** Distribution of mean baseline sound response amplitudes for all sound responsive neurons.

Regularity of context modulates novelty response

Most neurons in AC that we imaged exhibited a novelty response: 55% of neurons exhibited a stronger response to the novel ripple in either the RND or REG condition as compared to the tuning response (significant change in mean response within the 300 ms window post-stimulus onset to the novel ripple compared to tuning response to that ripple). While novelty responses were greater than baseline sound responses to the same ripple on average (post-hoc Tukey-Kramer, $p < 1e-9$), there was no difference between the mean response in the REG and RND contexts over the entire population (post-hoc Tukey-Kramer, $p=0.18$). However, these changes were significant when computed separately for the positive ($n = 2,832$) and negative ($n = 2,202$) responding neurons (Figure 2 B, C). The remaining neurons ($n = 4,092$) exhibited no significant difference in response to the novel ripple compared to its baseline response (Figure 2D).

Importantly, for either positive or negative responses, the REG context enhanced the novelty response in the corresponding direction. The novelty response magnitude was greater under the REG context than under the RND context (30.1%, post-hoc Tukey-Kramer, $p < 6.56e-$

7, for positive responses; 12.9%, post-hoc Tukey-Kramer, $p < 1e-10$, for negative responses). The context-dependent difference in novelty response strength was largest when we considered neurons with both positive novelty and baseline sound responses to the novel ripple (33.3%, repeated measures ANOVA, $p < 1e-10$, Figure 2E). These results are consistent with our predictions, as we expected the novelty response to be stronger in the regular compared to random conditions.

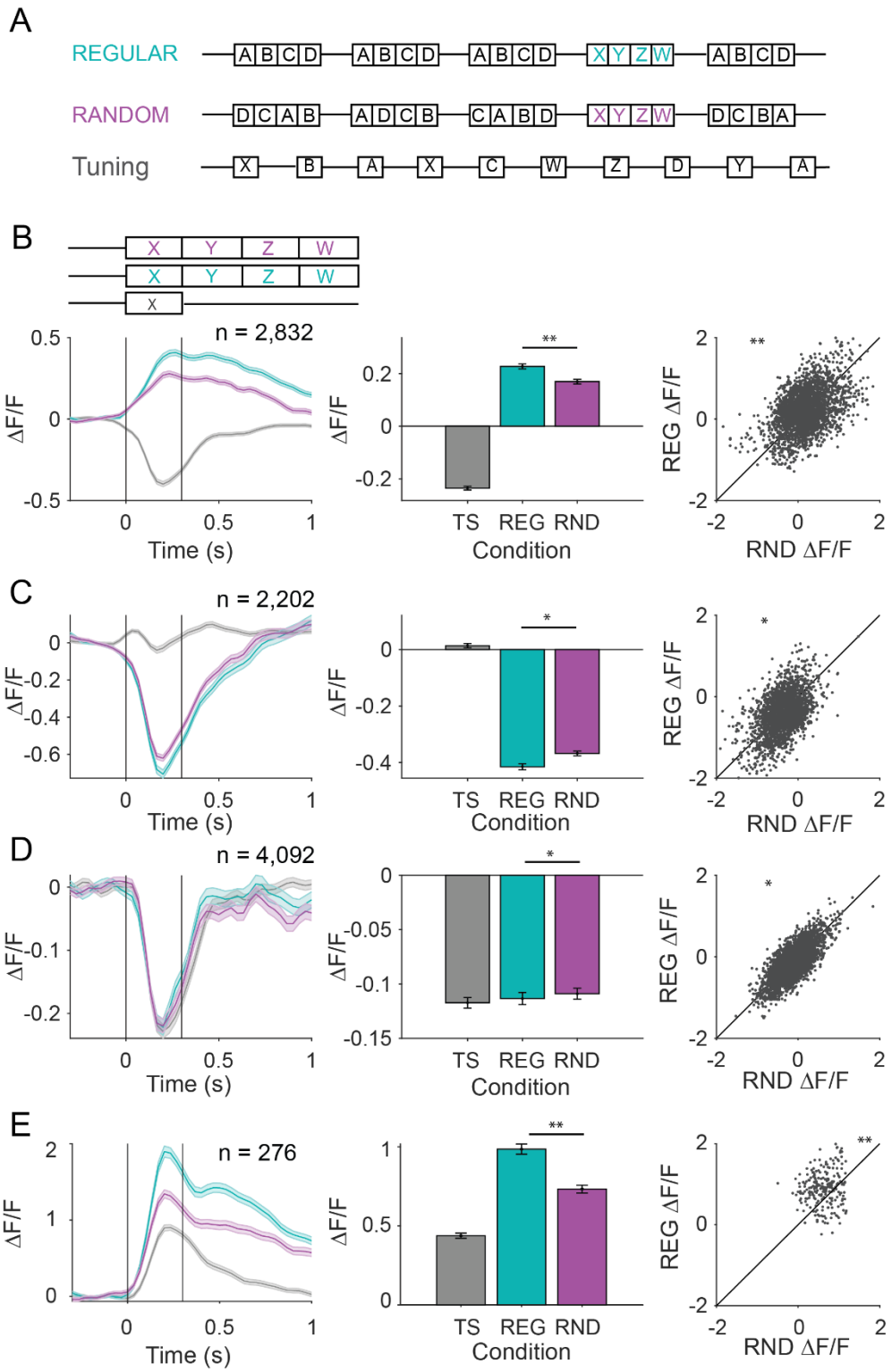

306

307 **FIGURE 2 AC neurons exhibit stronger novelty responses in regular than random contexts.**

a Schematic of the stimuli for REG and RND contexts (sequence of 4 ripples ABCD) with novel ripples (XYZW). A tuning stimulus comprising each of 8 ripples was used to identify the baseline sound response of ripple for individual neurons. **b** Population-averaged calcium traces across neurons with positive novelty response to the novel ripple presented in the REG context (cyan), RND context (purple), and as part of tuning stimulus (grey) as z-scored $\Delta F/F$ on the left. Vertical lines represent duration of the first novel ripple. Mean responses over 300 ms post stimulus onset for each of the three conditions shown in the middle. The mean responses show a significant effect of context on the response amplitude (repeated measures ANOVA: $p < 1e\text{-}10$) with REG responses being the largest, followed by RND, and then the baseline sound response (TS) (Tukey-Kramer post-hoc, $p < 6.56e\text{-}7$). The right panel shows the mean responses in the REG and RND context for individual neurons. **c** Average responses over all negative novelty responses (repeated measures ANOVA, $p < 1e\text{-}10$). For negative responses, average baseline response is the greatest, followed by RND, and then REG (post-hoc Tukey-Kramer, $p < 6.50e\text{-}6$). **d** Average responses over all neurons without a significant novelty response (repeated measures ANOVA, $p = 0.014$). While there was no significant difference between baseline and REG ($p = 0.62$) or RND ($p = 0.10$), there was a slight difference between REG and RND responses ($p = 0.02$) **e.** Average responses over all neurons with both a positive sound response and a positive novelty response (repeated measures ANOVA, $p < 1e\text{-}10$). REG responses are the greatest, followed by RND responses (post-hoc Tukey-Kramer, $p < 5.96e\text{-}8$).

We next analyzed how the novelty response changes over the course of an entire REG or RND stimulus block. Previous work has shown that adaptation in AC occurs over multiple time scales (Ulanovsky et al., 2004). We hypothesized that temporal regularity may also impact adaptation on longer time scales in a similar manner, with stronger adaptation occurring in the REG context compared to the RND context. We fit an exponential response function to the time course of per trial responses from individual neurons (Figure 3 B, E). We found that a sizeable fraction of neurons exhibited long term adaptation (48.03%) or facilitation (41.52%) to the novel ripple presentation. Neurons adapted faster in the REG as compared to RND context (Figure 3 D, G): time constants for both adaptation and facilitation were greater in the RND context than the REG context (2-way ANOVA, $f(1) = 10.29$, $p = 4.37e\text{-}3$), indicating that context has also has a secondary effect on the long-term adaptation of neuronal responses to the novel ripple. These results demonstrate a secondary mechanism for adaptation to stimulus context during novelty detection.

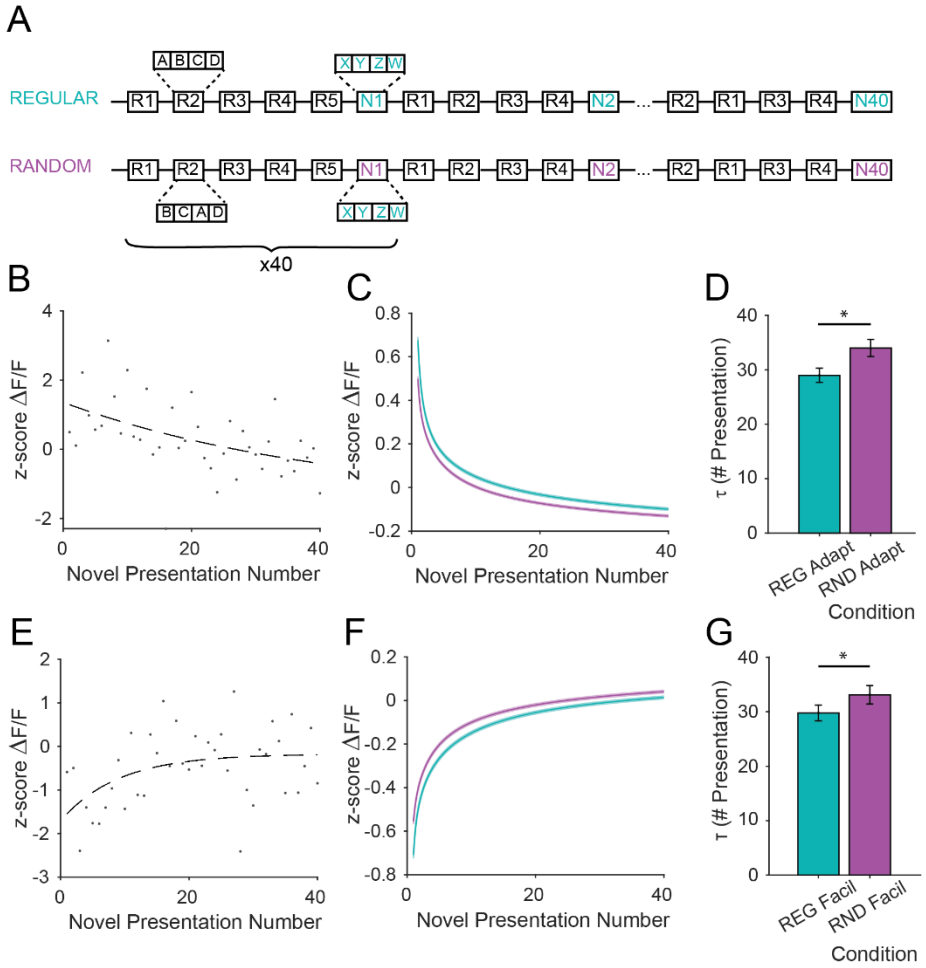

FIGURE 3 Temporal regularity modulates long term response dynamics
a Ripple sequences were presented in blocks of entire REG or RND contexts. The novel ripple is always the same, allowing for potential adaptation to the novel ripple itself. **b, e** Novelty responses over successive novel stimulus presentations for example cells exhibiting adaptation (b) and facilitation (e) in neuronal responses to the novel ripple sequence in a REG context. Dots are mean responses from an individual presentation of the ripple and the dashed line is the best exponential fit. **c,f** Exponential fits for adaptation and facilitation in REG (cyan) and RND (purple) contexts across the population. **d,g** Mean time constants for adaptation and facilitation in REG and RND contexts for all neurons that exhibit such long-term dynamics. Both adaptation and facilitation are faster in the REG context (2-way ANOVA, p = 4.37e-3).

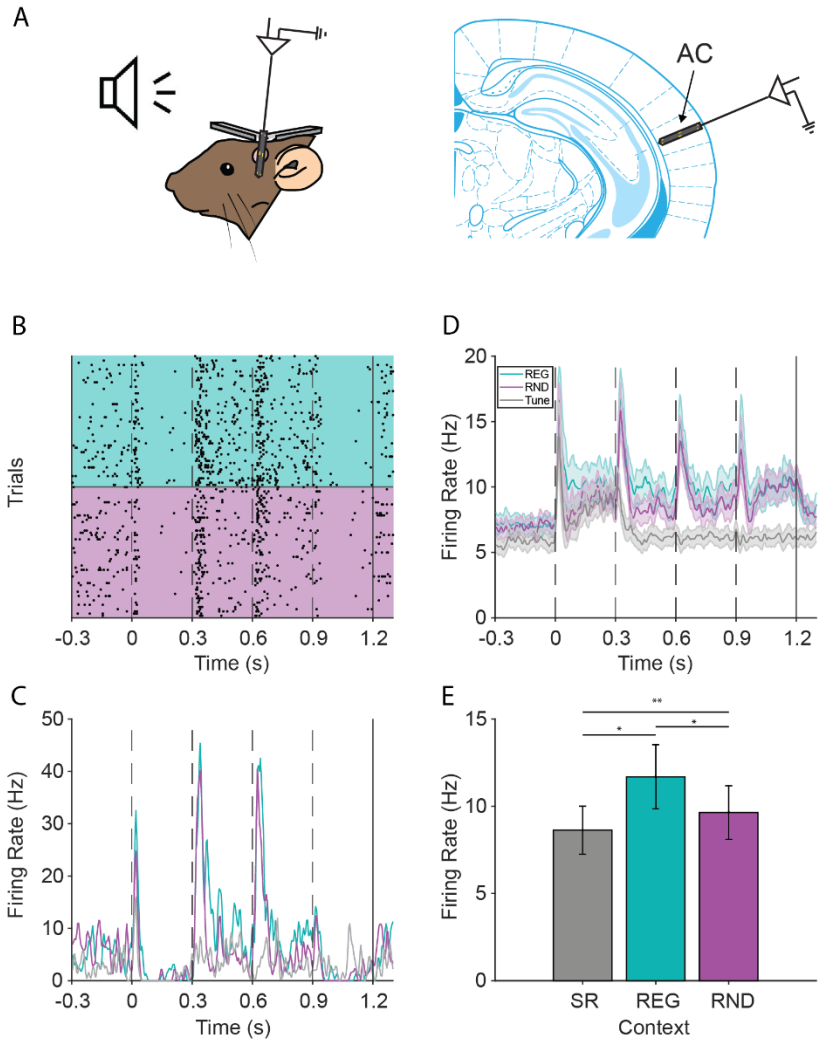

Figure 4 AC neurons exhibit higher firing rates to novel ripples in regular as compared to random contexts.

a Left: schematic of electrophysiological recording from AC in awake head-fixed mice. Right: Electrode superimposed on the AC outline from the Paxinos Brain Atlas (Paxinos and Franklin, 2012). **b**Raster plot of spike times from an example neuron in response to the novel ripple sequence in REG (cyan) and RND (purple) context. **c** PSTH of the same neuron's firing rate in response to the novel ripple sequence in REG and RND as well as the tuning response to the first ripple in the novel sequence (grey). **d** Mean firing rates over all neurons with a significant novelty response (n = 164) to the novel ripple sequence in REG (cyan), RND (purple), and to the first ripple in isolation (grey). **e** Mean firing rates in the first 100 ms post stimulus onset in REG, RND, and tuning contexts show a significant effect of context (repeated measures ANOVA, $f(2) = 9.36$, $p = 0.00012$). Error bars represent SEM.

Cortical neurons exhibit differential spiking responses to novel ripples in regular and random contexts

To resolve finer temporal information in cortical responses, we next performed electrophysiological recordings in the auditory cortex of awake mice (n = 5) while presenting the ripple stimuli (Figure 4 A-C). From these recordings, we identified novelty responsive units using a paired t-test between the spike rates from the 300 ms following stimulus onset when the ripple was presented in isolation versus as a deviant and found that most neurons exhibited a novelty response in either context (55%, n = 164 neurons). Among the units with a significant novelty response, 59% responded with an increase in firing rate (n = 96 neurons). When comparing the firing rates in response to the novel ripple in the REG and RND contexts, there was a significant effect of context in the first 100 ms of the response (Figure 4D, repeated measures ANOVA, $f(2) = 9.36$, $p = 0.00012$). Responses in the REG context were significantly greater than those in the RND context (post-hoc Tukey-Kramer, $p = 0.029$). Furthermore, the differential effect of context extended to the first 100 ms of the second (paired t-test, $p = 0.0166$) and third (paired t-test, $p = 0.0192$) ripples in the novel sequence but not the fourth (paired t-test, $p = 0.0928$). When examining the last 100 ms of the response to the first ripple, although the mean firing rate was higher in the REG context (~10.2 Hz) compared to the RND context (~9.2 Hz), there was no significant effect of context (repeated measures ANOVA, $f(2) = 2.022$, $p = 0.13$). These results indicate that the information about context is integrated early in the responses of neurons in AC and support our findings from 2-photon imaging.

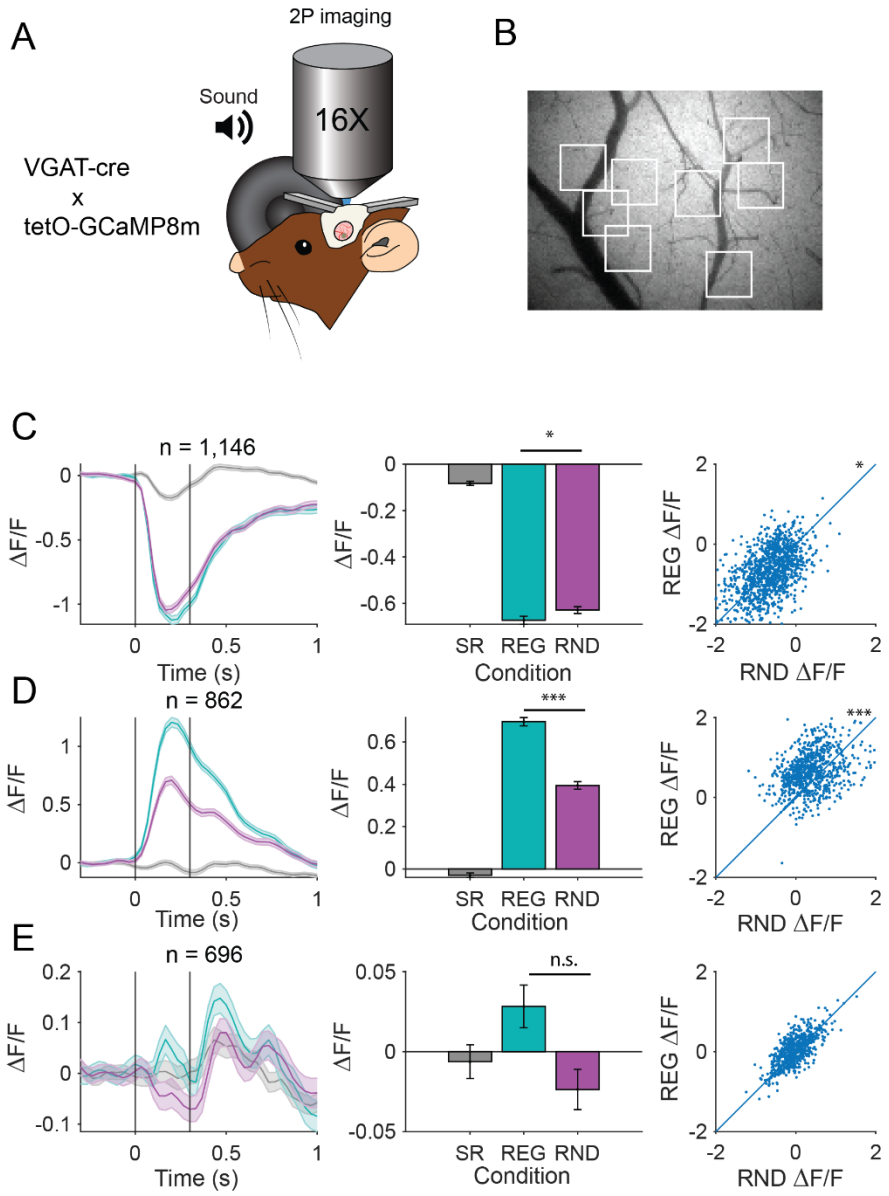

Figure 5. Inhibitory neurons in AC exhibit context-dependent novelty responses. **a** Schematic of 2-photon imaging from a transgenic mouse line expressing GCaMP8m only in inhibitory neurons. **b** Representative fields of view imaged (white boxes) overlayed on auditory cortex. For clarity, imaging areas close to one another have been combined. **c** Average responses over all negative novelty responses (repeated measures ANOVA, p = 1.59e-39). For negative responses, REG novelty responses were significantly lower than RND responses (post-hoc Tukey-Kramer, p = 2.27e-5) **d** Average responses over all positive novelty responses (repeated measures ANOVA, p = 3.14e-24). For positive responses, REG novelty responses are significantly greater than RND novelty responses (post-hoc Tukey-Kramer, p = 2.69e-5). **e** Average responses of all neurons without a significant novelty response (ANOVA, p = 0.98).

Cortical inhibitory neurons exhibit contextually modulated novelty responses

Inhibitory neurons modulate novelty responses in AC (Natan et al., 2015; Yarden et al., 2022) as well as other sensory areas (Millman et al., 2020; Furutachi et al., 2024). In AC, cortical inhibitory neurons also exhibit the enhanced deviance response associated with SSA (Natan et al., 2015). We investigated whether cortical inhibitory neurons exhibit a similar novelty response to our ripple stimulus by imaging from a VGAT-Cre mouse line crossed with a transgenic cre-dependent GCaMP8m line. This crossed line results in GCaMP8m expression only in inhibitory neurons. We found that, similar to our results from our pan-neuronal recordings, inhibitory neurons also exhibit a context-modulated novelty response (Figure 5). We found that 74.3% of cortical inhibitory neurons exhibited a significant novelty response. While the REG context enhances the response compared to the RND context for positive responses (72.2%, post-hoc Tukey-Kramer, $p = 3.14e-24$), negative responses in the REG context are lower than the RND (post-hoc Tukey-Kramer, $p = 2.27e-5$) (Figure 5 C, D). Furthermore, in contrast to the general population of neurons, the inhibitory neuronal population that did not exhibit a significant novelty response did not show a strong suppressive sound response (Figure 5E). The larger fraction of novelty sensitive inhibitory neurons and relatively smaller sound responses indicate that the novelty response found in the general population may be controlled by inhibitory neurons.

Optogenetic inactivation of inhibitory neurons differentially modulates novelty responses

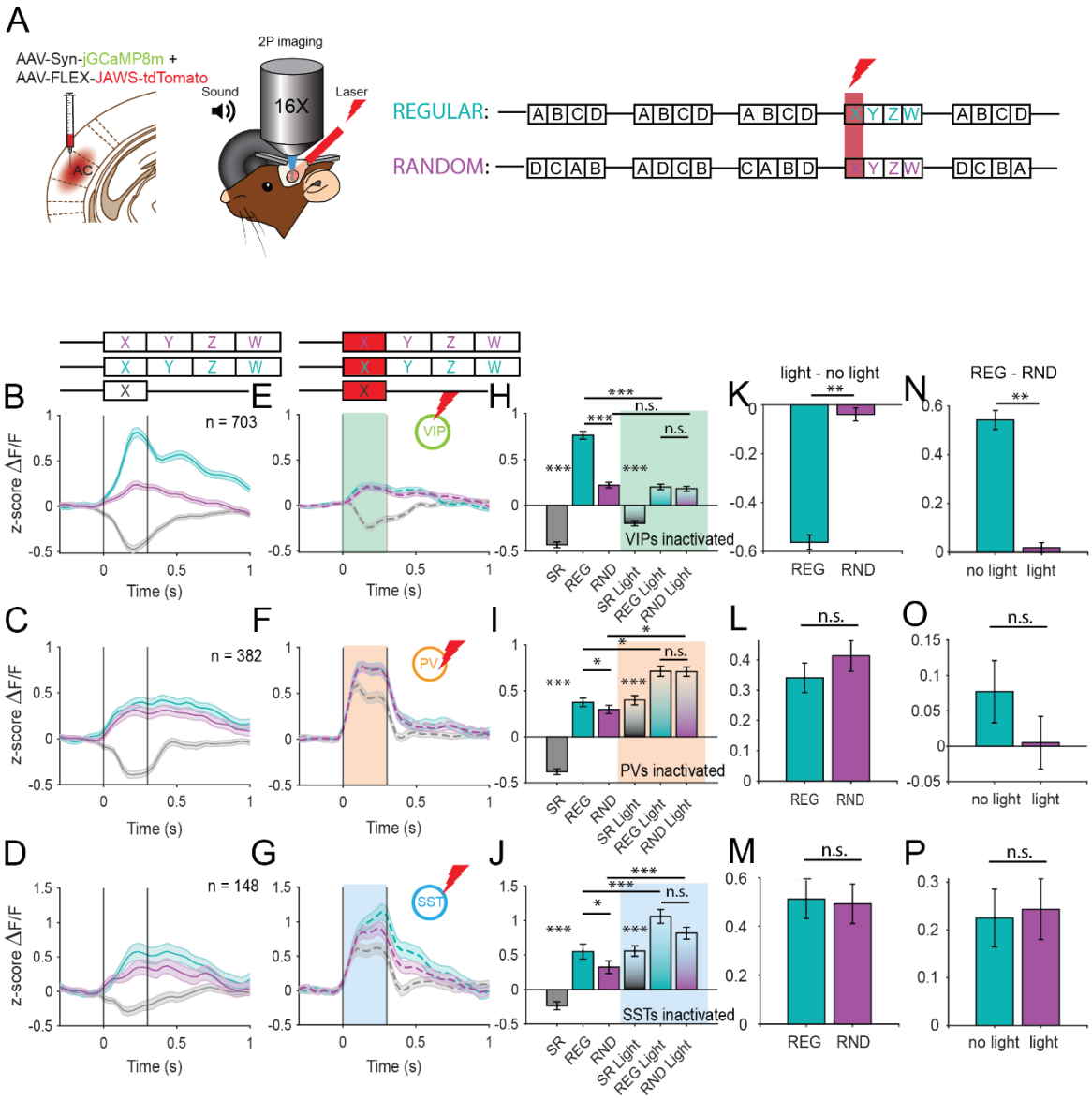

FIGURE 6 Selective context-dependent modulation of novelty responses by VIP neurons. **a** Diagram of the imaging and optogenetic manipulation set-up. Left: image from the Paxinos Brain atlas (Paxinos and Franklin, 2012) with the injection of the GCamP and Jaw virus targeted to A1. 2-photon imaging was performed in mice injected with JAWS-tdTomato in addition to GCaMP. Optogenetic inactivation was performed during the first ripple in the novel sequence. **b,e,h,k,n** Population averaged calcium trace (left panel) for novelty responses in the REG/RND context (cyan/purple) with and without optogenetic light stimulation (solid/dashed lines) to inhibit VIP neurons. Black line represents the baseline sound response. Only neurons with a significant light response are included. Mean activity in the 300 ms post stimulus onset is shown in the middle panel. Inactivation of VIP neurons reduces the novelty response (2-way repeated measures ANOVA, p = 3.43e-22). Furthermore, the inactivation results in a differential modulation of the

novelty response, with a much larger reduction in activity for the REG response than the RND response (2-way repeated measures ANOVA, $p = 3.077e-18$). Right panels show the light effect (with light – without light) for individual neurons, and the effect of context (REG – RND) in trials with and without light. Neurons responsive to VIP inactivation did exhibit a significant baseline sound response with (t-test, $p < 1e-10$) and without (t-test, $p = 4.11e-9$) light. **c,f,i,l,o** Inactivation of PV neurons increases the novelty response (2-way repeated measures ANOVA, $p = 4.30e-23$) and does not result in a differential effect between the REG and RND conditions (2-way repeated measures ANOVA, $p = 0.22$). Neurons responsive to PV inactivation did exhibit a significant baseline sound response with (t-test, $p = 2.13e-29$) and without (t-test, $p = 2.81e-23$) light. **d,g,j,m,p** Similar plots for SST inactivation. Optogenetic inactivation of SST cells also increases the novelty response (2-way repeated measures ANOVA, $p < 1.056e-12$) but does not result in a differential effect (2-way repeated measures ANOVA, $p = 0.49$). Neurons responsive to SST inactivation did exhibit a significant baseline sound response with (t-test, $p = 7.61e-11$) and without (t-test, $p = 1.13e-13$) light.

We next asked how specific classes of inhibitory neurons modulate cortical novelty detection in different contexts. Previous work has shown that PV and SST neurons differentially modulate stimulus-specific and temporal adaptation in AC (Natan et al., 2015, 2017). VIP neurons form a disinhibitory circuit with SST neurons and have also been shown to modulate novelty responses in sensory cortex (Furutachi et al., 2024). Therefore, we hypothesized that these distinct inhibitory neuron classes differentially modulate novelty responses in regular and random contexts. To investigate the role of inhibitory neurons in modulating the novelty response, we measured calcium activity in AC neurons while inactivating PV, SST, or VIP neurons using optogenetic activation of JAWS on a subset of trials (Figure 6A). JAWS is a red-shifted inhibitory opsin[27] which we expressed selectively in each of three interneuron subtypes using Cre-expressing transgenic mice. We inactivated each of the three inhibitory neuron classes during the presentation of the first ripple in the novel sequence to identify their selective role in modulating the response. As expected, inactivating VIP neurons decreased responses to ripples, whereas inactivating SST or PV neurons increased the responses to ripples (Figures 6 B-P; 7 B-P, gray solid and dashed lines).

For neurons with a positive novelty response, inactivation of VIP neurons decreased the amplitude of tuning response to the ripples (paired t-test, $p = 2.59e-28$, Figure 6 B, E, H). The effect of VIP neurons on novelty responses was selective for the temporal context (2-way repeated measures ANOVA, p (Context x Light) = 3.08e-18, Figure 6 B, E, H, K, N): suppressing VIP neurons significantly reduced novelty response in the regular (post-hoc Tukey-Kramer, $p < 1e-10$, Figure 6 E, H), but not random contexts (post-hoc Tukey-Kramer, $p = 0.76$ Figure 6 E, H, K). Furthermore, VIP inactivation resulted in the REG novelty response being similar in magnitude to the RND response, abolishing the context-dependent difference in novelty responses (post-hoc Tukey-Kramer, $p = 0.06$, Figure 6H). Inactivating PV or SST neurons increased tuning responses to the ripple, changing the mean response from negative to positive (paired t-test, $p_{PV} < 1e-20$, $p_{SST} = 2.74e-21$, Figure 6 C, F, I, D, G, J). Inactivating PV or SST neurons increased the novelty response for both REG (post-hoc Tukey-Kramer, $p_{PV} < 1e-10$, Figure 6 C, F, I, $p_{SST} = 1.06e12$, Figure 6 D, G, J) and RND (post-hoc Tukey-Kramer, $p_{PV} < 1e-10$, Figure 6 C, F, I, $p_{SST} = 0.0083$, Figure 6 D, G, J) contexts. However, there was no difference in the increase in novelty response due to the temporal context (2-way repeated measures ANOVA, p_{PV} (Context x Light) = 0.22, Figure 6 I, L, O, p_{SST} (Context x Light) = 0.48, Figure 6 J, M, P). Thus, VIP neurons selectively control the novelty responses in REG, but not RND context, whereas PV and SST neurons reduce novelty responses in a context-independent fashion.

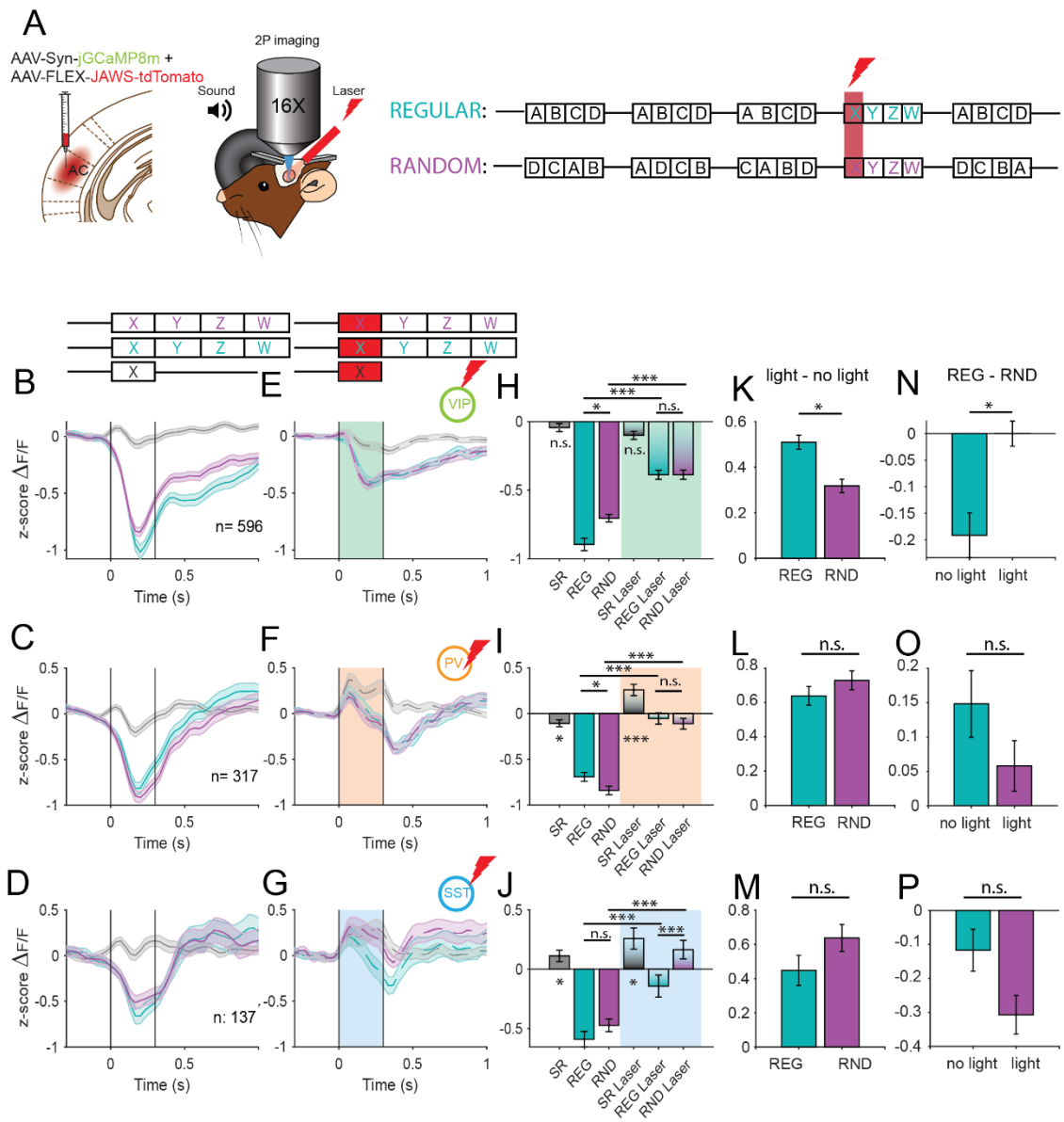

Figure 7. Neurons with a negative novelty response exhibit differential effects under optogenetic inactivation of three types of inhibitory neuron classes.
a Same format as Figure 6. **b,e,h,k,n** Effects of optogenetic inactivation of VIP neurons on neurons with a negative novelty response. VIP inactivation also increases novelty responses (2-way repeated measures ANOVA, $p < 1e\text{-}10$) while differentially modulating responses based on context (2-way repeated measures ANOVA, $p = 0.037$). Neurons responsive to VIP inactivation did not exhibit a significant baseline sound response with (t-test, $p = 0.16$) and without (t-test, $p = 0.93$) light. **c,f,i,l,o** Inactivation of PV neurons increased negative responses (2-way repeated measures ANOVA, $p = 5.51e\text{-}41$), but exhibited no differential effect (2-way repeated measures ANOVA, $p = 0.54$). Neurons responsive to PV inactivation did exhibit a significant baseline sound response with (t-test, $p = 0.0061$) and without (t-test, $p = 5.33e\text{-}6$) light. **d,g,j,m,p** Inactivation of SST

neurons increased novelty response (2-way repeated measures ANOVA, $p = 6.021e-14$, but not differentially based on context (2-way repeated measures ANOVA, $p = 0.13$). Neurons responsive to SST inactivation did exhibit a significant baseline sound response with (t-test, $p = 0.0012$) and without (t-test, $p = 0.015$) light.

For neurons that have negative novelty responses, optogenetic inactivation of all three interneuron classes increased the activity during the novel stimulus (Figure 7). Inactivating VIP neurons had no effect on the tuning responses (paired t-test, $p = 0.097$, Figure 7 B, E, H). For novelty responses, inactivating VIP neurons decreased the novelty responses under both random and regular contexts (2-way repeated measures ANOVA, $p < 1e-20$,Figure 7 B, E, H, K). However, this modulation of novelty responses was context-dependent, with stronger effect for regular as compared to random context (2-way repeated measures ANOVA, p(Context x Light) = 0.037, Figure 7 K, N), as context-dependent difference in novelty responses was abolished (Figure 7N). Inactivating PV neurons increased tuning responses to ripples (paired t-test, $p = 8.10e-9$ Figure 7 C, F, I) while inactivating SST neurons did not (paired t-test, $p = 0.19$SST Figure 7 D, G, J). For novelty responses, inactivating PV and SST neurons increased the novelty responses under both regular and random contexts (2-way repeated measures ANOVA, $p_{PV} = 5.51e-41$, Figure 7 C, F, I, L; $p_{SST} = 6.021e-14$, Figure 7 D, G, J, M). This change in novelty response was not context-dependent for either PV or SST neuron inactivation (PVs: 2-way repeated measures ANOVA, $p = 0.54$, Figure 7 L, O; SSTs: 2-way repeated measures ANOVA, $p = 0.13$, Figure 7 M, P). These results further support the differential function of VIP, but not SST or PV neurons under different contexts. The difference in effects for negative as compared to positive novelty responses indicates that negative novelty responses may be driven by different neural circuitry as compared to positive responses.

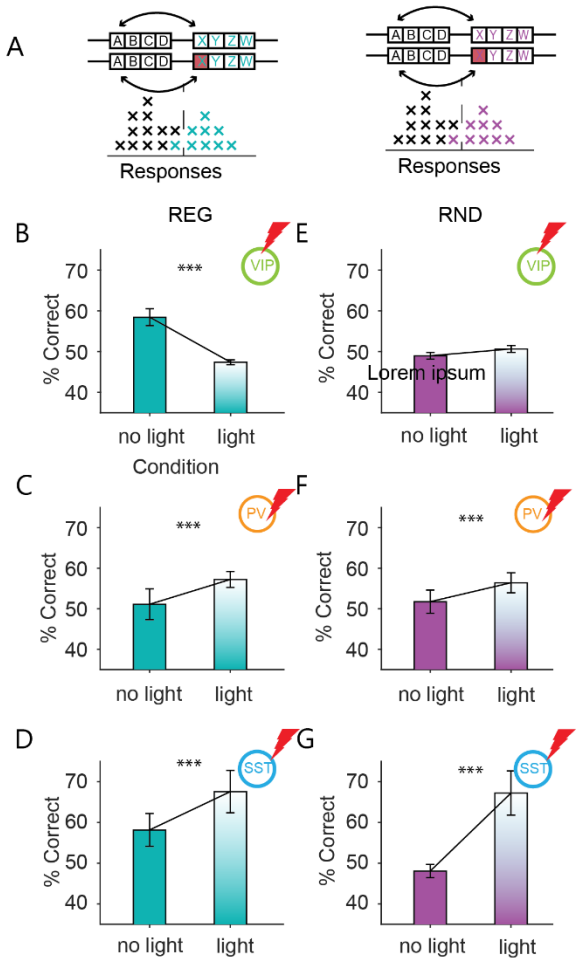

Figure 8 Differential effect of inhibitory neuronal inactivation on novelty detection under random and regular contexts.
a Schematic of SVM classification for single neurons. The activity during individual presentations of the a context ripple and the novel ripple X was used to train the classifier under regular and random context and during light and no light trials. **b,c,d** Single neuron SVM performance for trials with and without light in the REG context. VIP inactivation decreased SVM performance (post-hoc Tukey-Kramer, $p = 0.00036$), whereas PV (post-hoc Tukey-Kramer, $p < 7.76e-7$) and SST inactivation (post-hoc Tukey-Kramer, $p < 1.28e-7$) improved SVM performance. **e,f,g** Same plots for responses in RND context VIP inactivation had no effect (post-hoc Tukey-Kramer, $p = 0.85$), whereas PV (post-hoc Tukey-Kramer, $p = 0.00017$) and SST inactivation (post-hoc Tukey-Kramer, $p < 4.99e-9$) increased SVM performance.

To understand how, across the positive and negative novelty responses, the inhibitory neurons affected novelty detection, we trained a support vector machine (SVM) classifier to differentiate between a novel ripple and a context ripple (Figure 8A). For each recording session, we trained

the classifier on the responses to the novel ripple X versus responses to the first ripple in the repeated background sequence. To match the position in the sequence, we used the last repeat prior to the novel ripple on each trial. For regular contexts, this was always A, whereas for random contexts, this ripple varied between A, B, C and D. We compared the performance of the classifier in predicting whether neuronal responses corresponded to the novel or context ripple for trials with light (when the inhibitory neurons were suppressed) and without light, for the three different inhibitory neuron types.

We found that inactivating VIP neurons differentially modulated the classifier performance, reducing it only for the regular context condition, but not for the random context (post-hoc Tukey-Kramer, $p_{REG} < 0.00036$, post-hoc Tukey-Kramer, $p_{RND} < 0.85$, Figure 8 B, E). Inactivating PV or SST neurons improved SVM performance under both random (post-hoc Tukey-Kramer, $p_{PV} < 0.00017$, post-hoc Tukey-Kramer, $p_{SST} < 4.99e-9$, Figure 8 F, G) and regular (post-hoc Tukey-Kramer, $p_{PV} < 7.76e-7$, post-hoc Tukey-Kramer, $p_{SST} < 1.28e-7$, Figure 8 C, D) contexts. These results are in line with the changes in the mean response strength that we observed. They furthermore suggest that the selective effects of inactivating VIP neurons for REG context persist for discriminability of novel stimuli, whereas PV and SST neurons affect novelty responses, but not in a context-independent fashion.

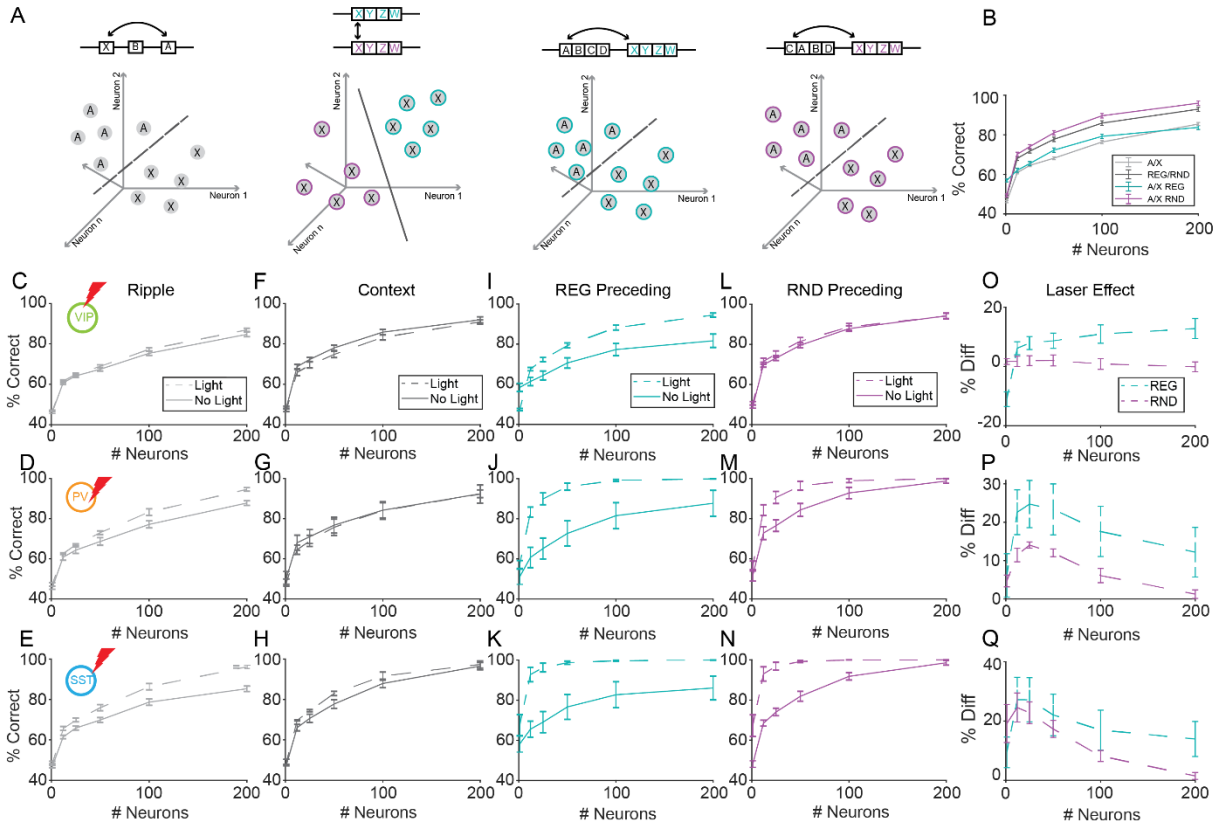

Figure 9 Population level representation of context is encoded more efficiently than stimulus identity

a Schematic of a SVM identifying a linear decision boundary between points in a high dimensional space. We computed the SVM to discriminate between ripples A and X from the tuning response stimulus; for the novel ripple X under REG and RND contexts; for the novel ripple X versus background context ripple under REG and RND contexts. All SVMs were trained and tested on data with and without optogenetic inactivation each of the three inhibitory neuronal classes.

b SVM discrimination performance between context ripple and novel ripple X from the sound response stimulus (grey) and discrimination performance between REG and RND contexts using the novelty response (black). Context is easier to classify than ripple identity (2-way ANOVA, f(1)=196.25, p=9.38e-33)

c,d,e Effect of optogenetic inactivation of VIP (top), SST (middle), and PV (bottom) neurons on ripple discrimination. Lines represent classifier performance, solid: trials without light, dashed: trials with light. Inactivation of VIP (2-way ANOVA, f(1) = 7.45, p = 0.0072), PV (2-way ANOVA, f(1) = 27.50, p = 5.094e-6), and SST (2-way ANOVA, f(1) = 58.62, p = 1.98e-9) neurons all improved ripple discrimination performance.

f,g,h Effects of inactivation of PV (top), SST (middle), and VIP (bottom) neurons on context discrimination. VIP inactivation decreased classification performance (2-way ANOVA, f(1) = 10.058, p = 0.0019) while SST inactivation improved performance (2-way ANOVA, f(1) = 12.47,

p = 0.001), and PV inactivation did not have a significant effect (2-way ANOVA, f(1) = 0.67, p = 0.42).

i,j,k Effects of inactivation of VIP (top), SST (middle), and PV (bottom) neurons on discriminating background and novel ripples in the REG context. Both PV (2-way ANOVA, f(1) = 50.18, p < 1.26e-8) and SST neuronal inactivation (2-way ANOVA, f(1)=58.45, p < 2.05e-9) improved performance, while VIP neuronal inactivation decreased performance for single neurons (post-hoc Tukey-Kramer, p = 0.00036) but increased performance over the population of neurons (2-way ANOVA, f(1) = 20.54, p < 1.26e-5).

l,m,n Effects of inactivation of VIP (top), SST (middle), and PV (bottom) neurons on discriminating background and novel ripples in the RND context. Both PV (2-way ANOVA, f(1) = 29.35, p < 2.91e-6) and SST neuronal inactivation (2-way ANOVA, f(1) = 75.31, p < 7.93e-9) enhances performance, while VIP neuronal inactivation had no effect on classification performance (2-way ANOVA, f(1) = 3.02, p = 0.085).

o,p,q Difference between classification performance with and without light inactivation for panels i-n

We next asked more broadly how these changes in novelty detection are implemented across the population of AC neurons. We expanded the discriminability analysis to multiple discrimination schemes and used subsets of progressively increasing number of neurons to train the SVMs. We found that discriminability increased with the number of neurons in the analysis and did not saturate at 200 neurons for either discrimination scheme (Figure 9B).

First, to establish a baseline in ripple discriminability based on the tuning stimulus, we computed the effect of inactivation of inhibitory neurons on discriminability between two ripples (Figure 9A left). PV and SST inactivation led to an increase in ripple discriminability, reaching higher than 90% discriminability at n = 200 neuron population size (2-way ANOVA, f(1) = 27.50, p_{PV} = 5.094e-6, Figure 9D; 2-way ANOVA, f(1) = 58.62, p_{SST} = 1.98e-9, Figure 9E).VIP inactivation has a significant, but much weaker effect (2-way ANOVA, f(1) = 7.45, p = 0. 0072, Figure 9 C, D, E). These results are consistent with prior studies that found that PV and SST neurons affect neuronal tuning properties (Aizenberg et al., 2015; Li et al., 2015; Natan et al., 2015, 2017; Phillips and Hasenstaub, 2016; Kato et al., 2017; Phillips et al., 2017), whereas VIP neurons have an inconsistent effect on tuning in AC (Mesik et al., 2015; Tobin et al., 2024).

Next, we compared the SVM performance on discriminating the novelty response under REG versus RND contexts. If VIP neurons play a selective role in providing context-dependent information, we expected that their inactivation would impair discriminability of novelty response across REG and RND contexts. By contrast, for PV and SST neurons, we expected that their inactivation would have little effect on context discriminability. Indeed, we found that inactivating VIP neurons impaired context discriminability of novelty responses, which is consistent with a decrease in difference in novelty responses under the two contexts (2-way ANOVA, $f(1) = 10.058$, $p = 0.0019$, Figure 9F). PV inactivation did not have a significant effect on context discriminability, whereas SST inactivation improved the discriminability performance (2-way ANOVA, $f(1) = 12.47$, $p = 0.001$, Figure 9 G, H).

Finally, we asked whether novelty detection under the two contexts improved with inhibitory neuronal inactivation. Surprisingly, we found that at a population level, inactivating all inhibitory neuron classes -- VIP, SST and PV neurons -- improved novelty detectability in REG context (2-way ANOVA, $f(1) = 20.54$, $p_{VIP} < 1.26e-5$, 2-way ANOVA, $f(1) = 50.18$, $p_{PV} < 1.26e-8$, 2-way ANOVA, $f(1)=58.45$, $p_{SST} < 2.05e-9$, Figure 9 I, J, K). In RND context, VIP inactivation did not have an effect, whereas SST or PV inactivation also drove an improvement in novelty detection (2-way ANOVA, $f(1) = 29.35$, $p_{PV} < 2.91e-6$, 2-way ANOVA, $f(1) = 75.31$, $p_{SST} < 7.93e-9$, Figure 9 L, M, N). The effect PV or SST inactivation was strongest around a population of $n = 10-25$ neurons (Figure 9 P, Q), suggesting that just a relatively small number of neurons can be involved in novelty detection. By contrast, effect of VIP inactivation on novelty detection in REG context increased with increasing number of neurons (Figure 9O), suggesting that VIP neurons transmit the information about context to larger cortical populations. The finding that novelty detection at population level is strongest when any of the three inhibitory neuron types are intact

suggest that the cortical circuits operate in suboptimal regime in everyday hearing, potentially allowing for context-dependent modulation by different inhibitory neuronal classes (Tobin et al., 2024).

DISCUSSION

In this study, we investigated how statistical regularity in sound sequences influences cortical responses to novel auditory stimuli, and how inhibitory neurons contribute to this process. Using calcium imaging and optogenetic inactivation in awake mice, we found that auditory cortex (AC) neurons exhibited stronger novelty responses when novel sounds followed a regular context compared to a random one. This enhancement was not uniform across cell types: while PV and SST interneuron inactivation broadly increased novelty responses with mixed effect of context, inactivation of VIP neurons selectively reduced responses in the regular context. These findings reveal a distinct role for VIP neurons in modulating context-dependent novelty detection in AC.

Our results align with human studies showing that novelty detection is enhanced by temporal predictability in sound streams. Previous EEG and behavioral work demonstrated that listeners respond more robustly to violations in regular versus random sequences, but the underlying neural circuitry was unknown (Barascud et al., 2016; Sohoglu and Chait, 2016; Southwell and Chait, 2018).. Here, by probing neuronal subtypes in mouse AC, we provide direct evidence for circuit-level modulation of novelty responses by context. Our results suggest that temporal regularity enhances novelty detection not merely by boosting adaptation or prediction error in individual neurons (Ulanovsky et al., 2003, 2004; Natan et al., 2015, 2017; Parras et al., 2017), but through targeted engagement of specific inhibitory networks.

A key contribution of this work is identifying VIP neurons as selective modulators of context-dependent novelty responses. While VIP neurons have been implicated in disinhibitory circuits across sensory cortical regions (Mesik et al., 2015; Pakan et al., 2016; Kuchibhotla et al., 2017; Cone et al., 2019; Millman et al., 2020; Myers-Joseph et al., 2024; Tobin et al., 2024) and have been implicated in oddball stimulus responses (Yarden et al., 2022), their role in encoding statistical structure in naturalistic auditory stimuli was previously untested. We show that VIP inactivation abolished the enhancement of novelty responses in the regular context without affecting responses in the random context. This selective effect suggests that VIP neurons integrate contextual information—potentially from top-down projections (Askew et al., 2019; Apicella and Marchionni, 2022; Ferguson et al., 2023) — to gate prediction error signaling (Friston and Kiebel, 2009; Friston, 2010; Heilbron and Chait, 2018). In contrast, PV and SST neurons modulate gain and adaptation more uniformly, regardless of context, consistent with their established roles in first-order sensory processing.

Our findings also have implications for how auditory scenes are represented at the population level. Using SVM-based decoding, we found that context information was more easily extracted from single-neuron responses in the regular condition, while population-level decoding performance plateaued more quickly. This shift toward a distributed, redundant code in regular contexts may reflect a network reorganization mediated by VIP neurons, as previously shown in auditory cortex (Tobin et al., 2024). Interestingly, inactivation of all interneuron types improved decoding of novel stimulus identity, suggesting that inhibition refines but also constrains the dynamic range of population responses.

One strength of our approach is the use of spectrally rich ripple stimuli, which elicit reliable responses in a broad population of AC neurons. These stimuli better approximate the complexity of natural sounds than pure tones and may engage higher-order auditory computations relevant to speech, communication, and environmental navigation. Our observation that deviance detection operates robustly across both excitatory and inhibitory populations reinforces the idea that prediction-related computations are a core function of auditory cortex.

This work also opens new questions about the origins of context signals that modulate VIP activity. VIP neurons are known to receive input from neuromodulatory and associative cortical areas, including prefrontal cortex (Kuchibhotla et al., 2017; Askew et al., 2019; Apicella and Marchionni, 2022; Ferguson et al., 2023; Ramamurthy et al., 2023),. The selectivity of VIP modulation for regular contexts may arise from top-down prediction signals that are absent in random sequences. Future studies using pathway-specific manipulations or recordings in interconnected regions will be needed to determine how these inputs shape VIP function (Furutachi et al., 2024).

Several caveats warrant consideration. First, while we focused on layer 2/3 pyramidal neurons, different interneuron subtypes span cortical layers and exhibit layer-specific functions. Our widefield optogenetic inactivation likely affected VIP, PV, and SST neurons in multiple layers, and the net effect observed in superficial recordings may reflect combined contributions from distinct circuits (Meyer et al., 2011; Tremblay et al., 2016; Yavorska and Wehr, 2016; Naka et al., 2019; Wu et al., 2022; David et al., 2023). Second, the precise nature of the statistical computations—adaptation versus prediction error—encoded by each subtype remains to be disentangled. Simultaneous recordings across AC layers and subcortical regions could further clarify how prediction errors are computed and propagated.

692 In summary, our study demonstrates that statistical context modulates novelty detection in auditory
693 cortex through specific inhibitory circuits. We identify VIP neurons as key players in shaping
694 prediction-error signals based on temporal structure. These findings support models of predictive
695 coding in sensory cortex and suggest that context-sensitive disinhibition is a fundamental
696 mechanism for flexible sensory processing. By revealing how different inhibitory neurons
697 contribute to novelty detection under structured versus random auditory regimes, our results
698 advance understanding of the neural basis of auditory perception in complex environments.

699

700

701 **Acknowledgements**

702 The authors would like to thank the members of the Geffen laboratory and Yale Cohen for their
703 discussions and helpful comments. This work was supported by the following grants from NIDCD:
704 R01DC15527, R01DC014479, R03DC013660, NINDS R01NS113241 to MNG. XD was
705 supported by T32DC016903.

Statistics Table.

Comparison	Figure	Test	N	Statistic	Effect Size	p-value
ANOVA for effects of REG/RND context on novelty response, all positive novelty responses	2b	One-way repeated measures ANOVA	2832	F(2)=1972.6	η2=0.411	<1e-10
Multiple comparison for REG, RND, and base sound response, all positive novelty responses	2b	post-hoc Tukey-Kramer	2832	MeanDifferenceBASEREG=-0.429 MeanDifferenceBASERND=-0.381 MeanDifferenceREGRND=0.0473	n/a	5.96e-08 5.96e-08 6.56e-07
ANOVA for effects of REG/RND context on novelty response, all negative novelty responses	2c	One-way repeated measures ANOVA	2202	F(2)=1543.1	η2=0.412	<1e-10
Multiple comparison for REG, RND, and base sound response, all negative novelty responses	2c	post-hoc Tukey-Kramer	2202	MeanDifferenceBASEREG=0.411 MeanDifferenceBASERND=0.366 MeanDifferenceREGRND=-0.0453	n/a	5.96e-08 5.96e-08 6.50e-06
ANOVA for effects of REG/RND context on novelty response, all non-significant novelty responses	2d	One-way repeated measures ANOVA	4092	F(2)=4.2832	η2=0.0010	0.014
Multiple comparison for REG, RND, and base sound response, all non-significant novelty responses	2d	post-hoc Tukey-Kramer	2202	MeanDifferenceBASEREG=0.0033044 MeanDifferenceBASERND=-0.0072995 MeanDifferenceREGRND=-0.010604	n/a	0.62 0.098 0.022

ANOVA for effects of REG/RND context on novelty response, positive novelty and sound response	2e	One-way repeated measures ANOVA	4092	F(2)=183.54	η2=.4003	<1e-10
Multiple comparison for REG, RND, and base sound response, positive novelty and sound response	2e	post-hoc Tukey-Kramer	276	MeanDifferenceBASEREG=-0.509 MeanDifferenceBASERND=-0.285 MeanDifferenceREGRND=0.224	n/a	5.96e-08 5.96e-08 5.96e-08
ANOVA for effects of REG/RND context and adaptation/facilitation on time constants	3d,g	Two-way ANOVA	8644	FREGRND(1)=8.1256 Fadaptfacil(1)=5.57e-6	η2=9.39e-4 η2=6.45e-10	0.0044 0.99
ANOVA for effect of context in novelty response for ephys	4d	repeated-measures anova	164	F(2)=9.3602	η2=0.0099598	0.00011
Multiple comparison for REG, RND, and base sound response, ephys	4d	post-hoc Tukey-Kramer	164	MeanDifferenceREGRND=0.0102 MeanDifferenceREGBASE=0.0153 MeanDifferenceRNDBASE=0.00507	n/a	0.024 0.0022 0.0091
ANOVA for effects of REG/RND context on novelty response, all negative novelty responses	5c	One-way repeated measures ANOVA	1146	F(2)=145.08	η2=0.5944	1.59e-39
Multiple comparison for REG, RND, and base sound response, all negative novelty responses	5c	post-hoc Tukey-Kramer	1146	MeanDifferenceBASEREG=0.701 MeanDifferenceBASERND=0.500 MeanDifferenceREGRND=-0.201	n/a	1.19e-07 1.19e-07 2.27e-05
ANOVA for effects of REG/RND context on novelty response, all	5d	One-way repeated	862	F(2)=72.02	η2=0.4211	3.14e-24

positive novelty responses		measures ANOVA				
Multiple comparison for REG, RND, and base sound response, all positive novelty responses	5d	post-hoc Tukey-Kramer	862	MeanDifferenceBASEREG=-0.558 MeanDifferenceBASERND=-0.304 MeanDifferenceREGRND=0.254	n/a	1.19e-07 1.19e-07 2.69e-05
ANOVA for effects of REG/RND context on novelty response, all non-significant novelty responses	5e	One-way repeated measures ANOVA	696	F(2)=0.020947	η2=0.9953	0.98
Multiple comparison for REG, RND, and base sound response, all non-significant novelty responses	5d	post-hoc Tukey-Kramer	862	MeanDifferenceBASEREG=-0.0019909 MeanDifferenceBASERND=-0.0047581 MeanDifferenceREGRND=-0.0027672	n/a	0.99 0.98 0.99
ANOVA for effects of context and optogenetic inactivation of VIPs on novelty responses	6h,k,n	2-way repeated measures anova	703	F(1)LIGHT=100.47 F(1)REGRND=101.78 F(1)Interaction=80.147	η2LIGHT=0.1313 η2REGRND=0.0991 η2Interaction=0.0115	3.43e-22 1.92e-22 3.077e-18
Multiple comparison for REG, RND, and base sound response, VIP optogenetic inactivation	6h	post-hoc Tukey-Kramer	703	MeanDifferenceRNDLIGHTNOLIGHT=-0.0057611 MeanDifferenceREGLIGHTNOLIGHT=-0.25717 MeanDifferenceLIGHTREGRND=-0.026605 MeanDifferenceNOLIGHTREGRND=-0.27802	n/a	0.76 <1e-10 0.056 <1e-10

ANOVA for effects of context and optogenetic inactivation of PVs on novelty responses	6i,l,o	2-way repeated measures anova	382	F(1)LIGHT=111.85 F(1)REGRND=3.657 F(1)Interaction=1.5165	η2LIGHT=0.0569 η2REGRND=7.3984e-04 η2Interaction=2.2624e-04	4.3e-23 0.057 0.22
Multiple comparison for REG, RND, and base sound response, PV optogenetic inactivation	6i	post-hoc Tukey-Kramer	382	MeanDifferenceRNDLIGHTNOLIGHT=-0.35848 MeanDifferenceREGLIGHTNOLIGHT=-0.31477 MeanDifferenceLIGHTREGRND=-0.060223 MeanDifferenceNOLIGHTREGRND=-0.01652	n/a	<1e-10 <1e-10 0.47 0.045
ANOVA for effects of context and optogenetic inactivation of SOMs on novelty responses	6j,m,p	2-way repeated measures anova	148	F(1)LIGHT=60.826 F(1)REGRND=7.1682 F(1)Interaction=0.48976	η2LIGHT=0.0729 η2REGRND=0.0028 η2Interaction=1.4091e-04	1.058e-12 0.0083 0.49
Multiple comparison for REG, RND, and base sound response, SOM optogenetic inactivation	6j	post-hoc Tukey-Kramer	148	MeanDifferenceRNDLIGHTNOLIGHT=-0.40566 MeanDifferenceREGLIGHTNOLIGHT=-0.37078 MeanDifferenceLIGHTREGRND=-0.093716 MeanDifferenceNOLIGHTREGRND=-0.05884	n/a	<1e-10 <1e-10 0.084 0.023
ANOVA for effects of context and optogenetic inactivation of VIPs on	7h,k,n	2-way repeated measures anova	703	F(1)LIGHT=565.43 F(1)REGRND=2.5212 F(1)Interaction=4.3612	η2LIGHT=0.0618 η2REGRND=4.4970e-04	<1e-10 0.11 0.037

negative novelty responses					η2Interaction=6.6104e-04	
Multiple comparison for REG, RND, and base sound response, VIP optogenetic inactivation	7h	post-hoc Tukey-Kramer	703	MeanDifferenceRNDLIGHTNOLIGHT=-0.27684 MeanDifferenceREGLIGHTNOLIGHT=-0.34419 MeanDifferenceLIGHTREGRND=-0.0071916 MeanDifferenceNOLIGHTREGRND=0.060159	n/a	<1e-10 <1e-10 0.65 0.036
ANOVA for effects of context and optogenetic inactivation of PVs on negative novelty responses	7i,l,o	2-way repeated measures anova	382	F(1)LIGHT=242.59 F(1)REGRND=6.3907 F(1)Interaction=0.37075	η2LIGHT=0.1508 η2LIGHT=0.0015 η2Interaction=5.0885e-05	5.51e-41 0.54
Multiple comparison for REG, RND, and base sound response, PV optogenetic inactivation	7i	post-hoc Tukey-Kramer	382	MeanDifferenceRNDLIGHTNOLIGHT=-0.58629 MeanDifferenceREGLIGHTNOLIGHT=-0.56467 MeanDifferenceLIGHTREGRND=-0.046523 MeanDifferenceNOLIGHTREGRND=-0.068141	n/a	<1e-10 <1e-10 0.056 0.037
ANOVA for effects of context and optogenetic inactivation of SOMs on negative novelty responses	7j,m,p	2-way repeated measures anova	148	F(1)LIGHT=70.144 F(1)REGRND=13.314 F(1)Interaction=2.3311	η2LIGHT=0.1381 η2REGRND=0.0065 η2Interaction=0.0011	6.021e-14 0.00037 0.13
Multiple comparison for REG, RND, and base sound response,	7j	post-hoc Tukey-Kramer	148	MeanDifferenceRNDLIGHTNOLIGHT=-0.52347 MeanDifferenceREGLIGHTNOLIGH	n/a	<1e-10 <1e-10

SOM optogenetic inactivation				T=-0.4363 MeanDifferenceLIGHTREGRND=-0.1473 MeanDifferenceNOLIGHTREGRND=-0.060134		3.33e-05 0.18
Multiple comparisons for SVM classification on RND background vs RND novel effects of light and population size with VIP inactivation	8e	post-hoc Tukey-Kramer	12	MeanDifference=-1.359	n/a	0.85
Multiple comparisons for SVM classification on RND background vs RND novel effects of light and population size with VIP inactivation	8f	post-hoc Tukey-Kramer	12	MeanDifference=-8.257	n/a	0.00017
Multiple comparisons for SVM classification on RND background vs RND novel effects of light and population size with VIP inactivation	8g	post-hoc Tukey-Kramer	12	MeanDifference=-15.581	n/a	4.98e-9
ANOVA for SVM classification performance on context and ripple identity	9b	2-way anova	20	Fpopsize(5)=519.13 Fcontextripple(1)=196.25	$\eta 2$=0.858 $\eta 2$=0.0649	4.12e-124 9.38e-33
ANOVA for SVM classification performance on background and novel	9b	2-way anova	20	Fpopsize(5)=106.91 Fregrnd1)=41.371	$\eta 2$=0.661 $\eta 2$=0.0511	2.70e-58 7.070e-10

in REG vs RND contexts						
Multiple comparisons for SVM classification REG vs RND no light	9b	post-hoc Tukey-Kramer	20	MeanDifference=-6.7395	n/a	7.30e-09
ANOVA for SVM performance on ripple identity in VIP mice	9c	2-way anova	12	Fpopsize(5)=548.12 Flightnolight(1)=7.4468	η2=0.950 η2=0.0026	1.077e-88 0.0072
ANOVA for SVM performance on ripple identity in PV mice	9d	2-way anova	4	Fpopsize(5)=284.2 Flightnolight(1)=27.503	η2=0.954 η2=0.0185	1.11e-30 5.094e-06
ANOVA for SVM performance on ripple identity in SST mice	9e	2-way anova	4	Fpopsize(5)=261.82 Fclass(1)=58.62	η2=0.929 η2=0.0291	5.66-30 1.98e-09
ANOVA for SVM performance on context identity in VIP mice	9f	2-way anova	12	Fpopsize(5)=296.12 Fclass(1)=10.058	η2=0.910 η2=0.0062	1.39e-71 0.0019
ANOVA for SVM performance on context identity in PV mice	9g	2-way anova	4	Fpopsize(5)=42.809 Fclass(1)=0.67358	η2=0.837 η2=0.0026	3.17e-15 0.42
ANOVA for SVM performance on context identity in SST mice	9h	2-way anova	4	Fpopsize(5)=258.65 Fclass(1)=12.465	η2= 0.960 η2=0.0093	7.21e-30 0.0010
ANOVA for SVM performance on background vs novel in REG in VIP mice	9i	2-way anova	12	Fpopsize(5)= 64.1 Fclass(1)=20.543	η2=0.671 η2=0.0430	3.49e-34 1.26e-05
ANOVA for SVM performance on background vs novel in REG in PV mice	9j	2-way anova	4	Fpopsize(5)=22.11 Fclass(1)=50.178	η2=0.548 η2=0.249	1.12e-10 1.27e-08

ANOVA for SVM performance on background vs novel in REG in SST mice	9k	2-way anova	4	Fpopsize(5)=12.54 Fclass(1)=58.452	 η2= 0.387 η2=0.361	2.056e-07 2.054e-09
ANOVA for SVM performance on background vs novel in RND in VIP mice	9l	2-way anova	12	Fpopsize(5)=265.13 Fclass(1)=3.016	 η2=0.9045 η2=0.0021	1.35e-68 0.085
ANOVA for SVM performance on background vs novel in RND in PV mice	9m	2-way anova	4	Fpopsize(5)=77.016 Fclass(1)=29.35	 η2=0.846 η2=0.0644	9.49e-20 2.90e-06
ANOVA for SVM performance on background vs novel in RND in SST mice	9n	2-way anova	4	Fpopsize(5)=46.278 Fclass(1)=75.309	 η2= 0.666 η2=0.217	8.36e-16 7.92e-11

Bibliography

Aizenberg M, Mwilambwe-Tshilobo L, Briguglio JJ, Natan RG, Geffen MN (2015) Bidirectional Regulation of Innate and Learned Behaviors That Rely on Frequency Discrimination by Cortical Inhibitory Neurons. PLoS Biology 13.

Antunes FM, Nelken I, Covey E, Malmierca MS (2010) Stimulus-specific adaptation in the auditory thalamus of the anesthetized rat. PloS one 5:e14071.

Apicella A junior, Marchionni I (2022) VIP-Expressing GABAergic Neurons: Disinhibitory vs. Inhibitory Motif and Its Role in Communication Across Neocortical Areas. Front Cell Neurosci 16 Available at: https://www.frontiersin.org/articles/10.3389/fncel.2022.811484 [Accessed April 26, 2024].

Arnal LH, Giraud A-L (2012) Cortical oscillations and sensory predictions. Trends in Cognitive Sciences 16:390–398.

Askew CE, Lopez AJ, Wood MA, Metherate R (2019) Nicotine excites VIP interneurons to disinhibit pyramidal neurons in auditory cortex. Synapse 73:e22116.

Attinger A, Wang B, Keller GB (2017) Visuomotor Coupling Shapes the Functional Development of Mouse Visual Cortex. Cell 169:1291-1302.e14.

Barascud N, Pearce MT, Griffiths TD, Friston KJ, Chait M (2016) Brain responses in humans reveal ideal observer-like sensitivity to complex acoustic patterns. Proceedings of the National Academy of Sciences 113:E616–E625.

Betzel RF, Wood KC, Angeloni C, Geffen MN, Bassett DS (2019) Stability of spontaneous, correlated activity in mouse auditory cortex. PLOS Computational Biology 15:e1007360.

Chen I-W, Helmchen F, Lütcke H (2015) Specific Early and Late Oddball-Evoked Responses in Excitatory and Inhibitory Neurons of Mouse Auditory Cortex. J Neurosci 35:12560–12573.

Chuong AS et al. (2014) Noninvasive optical inhibition with a red-shifted microbial rhodopsin. Nature neuroscience 17:1123.

Cone JJ, Scantlen MD, Histed MH, Maunsell JHR (2019) Different Inhibitory Interneuron Cell Classes Make Distinct Contributions to Visual Contrast Perception. eNeuro 6:ENEURO.0337-18.2019.

David F, Borel M, Ayub S, Ruther P, Gentet LJ (2023) Layer-specific stimulations of parvalbumin-positive cortical interneurons in mice entrain brain rhythms to different frequencies. Cereb Cortex 33:8286–8299.

Farley BJ, Quirk MC, Doherty JJ, Christian EP (2010) Stimulus-Specific Adaptation in Auditory Cortex Is an NMDA-Independent Process Distinct from the Sensory Novelty Encoded by the Mismatch Negativity. J Neurosci 30:16475–16484.

Ferguson KA, Salameh J, Alba C, Selwyn H, Barnes C, Lohani S, Cardin JA (2023) VIP interneurons regulate cortical size tuning and visual perception. Cell Rep 42:113088.

Friston K (2010) The free-energy principle: a unified brain theory? Nat Rev Neurosci 11:127–138.

Friston K, Kiebel S (2009) Predictive coding under the free-energy principle. Philosophical Transactions of the Royal Society B: Biological Sciences 364:1211–1221.

Furutachi S, Franklin AD, Aldea AM, Mrsic-Flogel TD, Hofer SB (2024) Cooperative thalamocortical circuit mechanism for sensory prediction errors. Nature 633:398–406.

Harms L, Fulham WR, Todd J, Budd TW, Hunter M, Meehan C, Penttonen M, Schall U, Zavitsanou K, Hodgson DM, Michie PT (2014) Mismatch Negativity (MMN) in Freely-Moving Rats with Several Experimental Controls. PLOS ONE 9:e110892.

Hattori R, Komiyama T (2022) PatchWarp: Corrections of non-uniform image distortions in two-photon calcium imaging data by patchwork affine transformations. Cell Reports Methods 2:100205.

Heilbron M, Chait M (2018) Great Expectations: Is there Evidence for Predictive Coding in Auditory Cortex? Neuroscience 389:54–73.

Hershenhoren I, Taaseh N, Antunes FM, Nelken I (2014) Intracellular correlates of stimulus-specific adaptation. The Journal of neuroscience : the official journal of the Society for Neuroscience 34:3303–3319.

Johnson KR, Tian C, Gagnon LH, Jiang H, Ding D, Salvi R (2017) Effects of Cdh23 single nucleotide substitutions on age-related hearing loss in C57BL/6 and 129S1/Sv mice and comparisons with congenic strains. Sci Rep 7:44450.

Kato HK, Asinof SK, Isaacson JS (2017) Network-Level Control of Frequency Tuning in Auditory Cortex. Neuron.

Kuchibhotla KV, Gill JV, Lindsay GW, Papadoyannis ES, Field RE, Sten TAH, Miller KD, Froemke RC (2017) Parallel processing by cortical inhibition enables context-dependent behavior. Nature neuroscience 20:62–71.

Lee S, Hjerling-Leffler J, Zagha E, Fishell G, Rudy B (2010) The Largest Group of Superficial Neocortical GABAergic Interneurons Expresses Ionotropic Serotonin Receptors. J Neurosci 30:16796–16808.

Lesicko AMH, Angeloni CF, Blackwell JM, De Biasi M, Geffen MN (2022) Corticofugal regulation of predictive coding. Elife 11:e73289.

Levy RB, Reyes AD (2012) Spatial Profile of Excitatory and Inhibitory Synaptic Connectivity in Mouse Primary Auditory Cortex. Journal of Neuroscience 32:5609–5619.

Li LY, Xiong XR, Ibrahim LA, Yuan W, Tao HW, Zhang LI (2015) Differential Receptive Field Properties of Parvalbumin and Somatostatin Inhibitory Neurons in Mouse Auditory Cortex. Cerebral cortex 25:1782–1791.

Malmierca MS, Anderson LA, Antunes FM (2015) The cortical modulation of stimulus-specific adaptation in the auditory midbrain and thalamus: a potential neuronal correlate for predictive coding. Front Syst Neurosci 9:19.

Mehra M, Mukesh A, Bandyopadhyay S (2022) Separate Functional Subnetworks of Excitatory Neurons Show Preference to Periodic and Random Sound Structures. J Neurosci 42:3165–3183.

Mesik L, Ma W, Li L, Ibrahim LA, Huang ZJ, Zhang LI, Tao HW (2015) Functional response properties of VIP-expressing inhibitory neurons in mouse visual and auditory cortex. Front Neural Circuits 9:22.

Meyer HS, Schwarz D, Wimmer VC, Schmitt AC, Kerr JND, Sakmann B, Helmstaedter M (2011) Inhibitory interneurons in a cortical column form hot zones of inhibition in layers 2 and 5A. Proceedings of the National Academy of Sciences 108:16807–16812.

Millman DJ, Ocker GK, Caldejon S, Kato I, Larkin JD, Lee EK, Luviano J, Nayan C, Nguyen TV, North K, Seid S, White C, Lecoq J, Reid C, Buice MA, de Vries SE (2020) VIP interneurons in mouse primary visual cortex selectively enhance responses to weak but specific stimuli Vinck M, Wassum KM, eds. eLife 9:e55130.

Myers-Joseph D, Wilmes KA, Fernandez-Otero M, Clopath C, Khan AG (2024) Disinhibition by VIP interneurons is orthogonal to cross-modal attentional modulation in primary visual cortex. Neuron 112:628-645.e7.

Naatanen R, Gaillard AW, Mantysalo S (1978) Early selective-attention effect on evoked potential reinterpreted. Acta psychologica 42:313–329.

Naatanen R, Paavilainen P, Rinne T, Alho K (2007) The mismatch negativity (MMN) in basic research of central auditory processing: a review. Clin Neurophysiol 118:2544–2590.

Naatanen R, Pakarinen S, Rinne T, Takegata R (2004) The mismatch negativity (MMN): towards the optimal paradigm. Clin Neurophysiol 115:140–144.

Naka A, Veit J, Shababo B, Chance RK, Risso D, Stafford D, Snyder B, Egladyous A, Chu D, Sridharan S, Mossing DP, Paninski L, Ngai J, Adesnik H (2019) Complementary networks of cortical somatostatin interneurons enforce layer specific control. Elife 8:e43696.

Natan RG, Briguglio JJ, Mwilambwe-Tshilobo L, Jones SI, Aizenberg M, Goldberg EM, Geffen MN (2015) Complementary control of sensory adaptation by two types of cortical interneurons. eLife 4:1–27.

Natan RG, Rao W, Geffen MN (2017) Cortical Interneurons Differentially Shape Frequency Tuning following Adaptation. Cell Reports 21:878–890.

Nelken I (2004) Processing of complex stimuli and natural scenes in the auditory cortex. Current opinion in neurobiology 14:474–480.

Nelken I (2014) Stimulus-specific adaptation and deviance detection in the auditory system: experiments and models. Biological cybernetics Available at: http://www.ncbi.nlm.nih.gov/pubmed/24477619.

Pachitariu M, Steinmetz N, Kadir S, Carandini M, D HK (2016) Kilosort: realtime spike-sorting for extracellular electrophysiology with hundreds of channels. :061481 Available at: https://www.biorxiv.org/content/10.1101/061481v1 [Accessed February 6, 2025].

Pachitariu M, Stringer C, Dipoppa M, Schröder S, Rossi LF, Dalgleish H, Carandini M, Harris KD (2017) Suite2p: beyond 10,000 neurons with standard two-photon microscopy. bioRxiv:061507.

Pakan JM, Lowe SC, Dylda E, Keemink SW, Currie SP, Coutts CA, Rochefort NL (2016) Behavioral-state modulation of inhibition is context-dependent and cell type specific in mouse visual cortex Mrsic-Flogel TD, ed. eLife 5:e14985.

Parras GG, Nieto-Diego J, Carbajal GV, Valdés-Baizabal C, Escera C, Malmierca MS (2017) Neurons along the auditory pathway exhibit a hierarchical organization of prediction error. Nat Commun 8:2148.

Paxinos G, Franklin KB (2012) The Mouse Brain in Stereotaxic Coordinates. Sydney: Academic Press.

Phillips EA, Hasenstaub AR (2016) Asymmetric effects of activating and inactivating cortical interneurons. eLife 5 Available at: https://www.ncbi.nlm.nih.gov/pubmed/27719761.

Phillips EAK, Schreiner CE, Hasenstaub AR (2017) Cortical Interneurons Differentially Regulate the Effects of Acoustic Context. Cell Rep 20:771–778.

Ramamurthy DL, Chen A, Zhou J, Park C, Huang PC, Bharghavan P, Krishna G, Liu J, Casale K, Feldman DE (2023) VIP interneurons in sensory cortex encode sensory and action signals but not direct reward signals. Current Biology 33:3398-3408.e7.

Rubin J, Ulanovsky N, Nelken I, Tishby N (2016) The Representation of Prediction Error in Auditory Cortex. PLoS Comput Biol 12:1005058.

Siegle JH, López AC, Patel YA, Abramov K, Ohayon S, Voigts J (2017) Open Ephys: an open-source, plugin-based platform for multichannel electrophysiology. J Neural Eng 14:045003.

Sohoglu E, Chait M (2016) Detecting and representing predictable structure during auditory scene analysis. eLife 5:1–17.

Solyga M, Keller GB (2025) Multimodal mismatch responses in mouse auditory cortex. eLife 13 Available at: https://elifesciences.org/reviewed-preprints/95398 [Accessed February 19, 2025].

Southwell R, Chait M (2018) Enhanced deviant responses in patterned relative to random sound sequences. Cortex 109:92–103.

Szymanski FD, Garcia-Lazaro JA, Schnupp JWH (2009) Current Source Density Profiles of Stimulus-Specific Adaptation in Rat Auditory Cortex. Journal of Neurophysiology 102:1483–1490.

Tobin M, Sheth J, Wood KC, Michel EK, Geffen MN (2024) Distinct inhibitory neurons differently shape neuronal codes for sound intensity in the auditory cortex. J Neurosci Available at: https://www.jneurosci.org/content/early/2024/11/06/JNEUROSCI.1502-23.2024 [Accessed December 16, 2024].

Tremblay R, Lee S, Rudy B (2016) GABAergic Interneurons in the Neocortex: From Cellular Properties to Circuits. Neuron 91:260–292.

Ulanovsky N, Las L, Farkas D, Nelken I (2004) Multiple time scales of adaptation in auditory cortex neurons. Journal of Neuroscience 24:10440–10453.

Ulanovsky N, Las L, Nelken I (2003) Processing of low-probability sounds by cortical neurons. Nature Neuroscience 6:391–398.

Vapnik V (2013) The Nature of Statistical Learning Theory. Springer Science & Business Media.

Vogler NW, Chen R, Virkler A, Tu VY, Gottfried JA, Geffen MN (2024) Direct Piriform-to-Auditory Cortical Projections Shape Auditory–Olfactory Integration. J Neurosci 44 Available at: https://www.jneurosci.org/content/44/49/e1140242024 [Accessed February 6, 2025].

Wood KC, Angeloni CF, Oxman K, Clopath C, Geffen MN (2022) Neuronal activity in sensory cortex predicts the specificity of learning in mice. Nature Communications 13.

Wood KC, Blackwell JM, Geffen MN (2017) Cortical inhibitory interneurons control sensory processing. Current Opinion in Neurobiology 46:200–207.

Wu J, Zhao Z, Shi Y, He M (2022) Cortical VIP+ Interneurons in the Upper and Deeper Layers Are Transcriptionally Distinct. J Mol Neurosci 72:1779–1795.

Yarden TS, Mizrahi A, Nelken I (2022) Context-Dependent Inhibitory Control of Stimulus-Specific Adaptation. J Neurosci 42:4629–4651.

Yaron A, Hershenhoren I, Nelken I (2012) Sensitivity to Complex Statistical Regularities in Rat Auditory Cortex. Neuron 76:603–615.

Yavorska I, Wehr MS (2016) Somatostatin-Expressing Inhibitory Interneurons in Cortical Circuits. Frontiers in Neural Circuits 10:1–18.